Frontiers in Bioscience Landmark

Front. Biosci. (Landmark Ed) **2026**; 31(8): 52385
https://doi.org/10.31083/FBL52385

Original Research

Multimodal Analysis Reveals Aberrant Expression of SUMO2 and Its Significant Association With Key Mechanisms of Metabolic Pathways in Hepatocellular Carcinoma

Yulong Deng[1,†], Beibei Huang[1,†], Yuxing Tang[2], Qinyan Su[2], Hongquan Liu[2], Hongbo Mo[2], Huanhuan Tang[2], Kunhua Xiong[2], Shipei He[2], Yiwu Dang[2], Gang Chen[2], Minhua Rong[1,*]

[1]Research Department, Affiliated Cancer Hospital, Guangxi Medical University, 530021 Nanning, Guangxi, China
[2]Department of Pathology, First Affiliated Hospital of Guangxi Medical University, 530021 Nanning, Guangxi, China
*Correspondence: tourtair@163.com (Minhua Rong)
[†]These authors contributed equally.

Academic Editor: Marco Falasca
Submitted: 29 March 2026 Revised: 6 July 2026 Accepted: 24 July 2026 Published: 18 August 2026

Abstract

Background: Hepatocellular carcinoma (HCC) is the third leading cause of cancer-related deaths worldwide. However, the role of small ubiquitin-like modifier 2 (SUMO2), a core member of the small ubiquitin-like modifier (SUMO) family, regarding its expression patterns and metabolism-related functions in HCC remains inadequately understood. **Methods:** A multidimensional analytical framework was applied, integrating immunohistochemistry (153 HCC vs. 21 non-HCC samples), proteomics (159 paired samples), bulk transcriptomics (3240 HCC vs. 2267 non-HCC samples), single-cell RNA sequencing (RNA-seq) (10 HCC vs. 8 non-HCC samples), spatial transcriptomics, and external CRISPR/Cas9 functional genomics data. Systematic analyses included standardized mean difference (SMD), pathway enrichment, pseudotime trajectory inference, *in silico* knockout, cell–cell communication, metabolic flux scoring, immune infiltration, clinical correlation, drug sensitivity prediction, and molecular docking. **Results:** At the protein level, immunohistochemistry (nuclear positivity) and external proteomic data collectively demonstrated consistent SUMO2 overexpression in HCC. Consistent upregulation was also observed at the mRNA level across large-scale cohorts. Single-cell RNA-seq and spatial transcriptomics localized SUMO2 enrichment to malignant hepatocytes and tumor-dominant regions. CRISPR-mediated SUMO2 knockout suppressed proliferation in multiple HCC cell lines. Mechanistically, high SUMO2 expression was significantly associated with metabolic reprogramming involving glycolysis/gluconeogenesis, pyruvate metabolism, and the tricarboxylic acid cycle. SUMO2-high malignant hepatocyte subpopulations exhibited enhanced activity of the macrophage migration inhibitory factor signaling axis and enhanced iron-sensor interactions. Further, the immune infiltration analysis revealed a negative correlation between SUMO2 expression and M1 macrophages and a positive correlation between follicular helper T cells and regulatory T cells. Clinically, elevated SUMO2 levels were found to be associated with adverse prognostic features. Furthermore, high SUMO2 expression was associated with increased sensitivity to dasatinib, and molecular docking simulations predicted potential binding between SUMO2 and dasatinib, with a Vina score of −8.5 kcal/mol. **Conclusions:** SUMO2 is aberrantly expressed at the protein, mRNA, single-cell, and spatial transcriptomic levels in HCC and is significantly associated with metabolic reprogramming and altered migration inhibitory factor (MIF)-mediated intercellular communication, suggesting its potential as a novel biomarker for diagnosis and treatment.

Keywords: hepatocellular carcinoma; small ubiquitin-like modifier 2; immunohistochemistry; single-cell RNA sequencing; spatial transcriptomics; metabolic reprogramming; macrophage migration inhibitory factor

1. Introduction

Hepatocellular carcinoma (HCC) represents the most prevalent subtype of primary liver cancer [1], ranking as the sixth most common malignant tumor worldwide and the third leading cause of cancer-related mortality [2]. Remarkable advances have been achieved in HCC therapeutics: hepatectomy has long served as the first-line therapeutic strategy [3], locoregional therapy forms the therapeutic cornerstone for patients with early to locally advanced disease [4], and the recent introduction of immune checkpoint inhibitor (ICI) combination regimens has markedly improved overall survival in patients with unresectable HCC [5]. Nonetheless, HCC typically presents with no specific clinical manifestations in its early stage, resulting in most patients being diagnosed only at an advanced stage. This clinical feature contributes to a persistent annual increase in HCC mortality by approximately 2–3% [6], and the prognosis remains dismal. Currently, alpha-fetoprotein (AFP) is the most commonly used serum biomarker for HCC, with a sensitivity and specificity of approximately 60% and 80%, respectively [7], which is far from meeting the requirements for accurate early diagnosis. It is thus paramount to advance

the precision diagnosis and treatment of HCC by identifying more reliable diagnostic and therapeutic biomarkers and elucidating their underlying molecular mechanisms [8].

Small ubiquitin-like modifier 2 (SUMO2) is a key member of the SUMO family. Through covalent modification of target proteins (i.e., SUMOylation), SUMO2 modulates protein stability, subcellular localization, protein–protein interactions, and transcriptional activity, thereby playing a central role in signal transduction across multiple diseases [9]. An increasing number of studies have recently revealed that elevated SUMO2 expression in HCC promotes tumor cell proliferation, migration, and invasion and modulates the cell cycle, thereby highlighting SUMO2's potential as a prognostic biomarker [10,11,12,13]. In addition, SUMO2 upregulation is linked to an immune mechanism wherein the inhibition of SUMOylation activates the type I interferon pathway and promotes dendritic cell maturation, thus enhancing the anti-tumor immune response [14]. SUMO2 also augments the stemness and tumorigenic potential of liver cancer stem cells (LCSCs) by stabilizing key proteins, including Flap Endonuclease 1(FEN1) and Acyl-CoA Synthetase Long-Chain Family Member 3 (ACSL3), and antagonizes erastin-induced ferroptosis, among other pleiotropic functional mechanisms [15,16]. Notably, aberrant metabolism constitutes one of the hallmarks of cancer, and the Warburg effect—whereby tumor cells preferentially undergo glycolysis and produce large amounts of lactate under aerobic conditions—represents a critical mechanism driving HCC progression [17,18,19]. However, existing studies have been largely confined to bulk mRNA expression profiling in small sample cohorts. A comprehensive characterization of SUMO2 expression at the large-scale, multi-center mRNA level, as well as its multi-dimensional localization at single-cell and spatial transcriptomic resolution, is lacking. Moreover, the computationally predicted links between metabolic reprogramming and the macrophage migration inhibitory factor (MIF) signaling pathway remain poorly defined.

In the present study, immunohistochemistry (IHC) was conducted on internal pathological tissue samples, proteomic profiling, multi-center, large-sample, multi-dimensional high-throughput sequencing datasets, and CRISPR knockout data were integrated to systematically evaluate the multi-dimensional expression of SUMO2 in HCC at the protein, mRNA, cellular, and spatial tissue levels. A suite of algorithms—including pathway enrichment, pseudotime trajectory analysis, *in silico* gene knockout, and cell–cell signaling interaction analysis—was innovatively employed to identify the potential regulatory mechanisms at the metabolic level. Furthermore, the correlations between the differential SUMO2 expression and the HCC immune microenvironment, survival prognosis, clinicopathological characteristics, and drug sensitivity were investigated in depth. Collectively, these analyses revealed that SUMO2 enhances crosstalk within the HCC-associated microenvironment by modulating metabolism- and MIF-related molecular mechanisms and computationally predicted SUMO2 as a potential novel diagnostic and therapeutic biomarker for HCC.

2. Materials and Methods

2.1 In-House Immunohistochemical Analysis

In total, 153 tissue microarrays (TMAs) of HCC tissues were purchased from Guilin Fanpu Biotechnology Co., Ltd. (TMA No.: LVC1531), with an additional 21 non-HCC liver tissue specimens collected from the First Affiliated Hospital of Guangxi Medical University. The samples were fixed in formalin, embedded in paraffin, and deparaffinized with ethylenediaminetetraacetic acid (EDTA) buffer. Endogenous peroxidase activity was then blocked, and the tissues were subsequently incubated at room temperature for 90 minutes with a rabbit monoclonal antibody against SUMO2 (Biorbyt Ltd., Cambridge, UK; Cat. No. orb136333; dilution 1:500). This was followed by incubation with HRP-labeled Poly-HRP anti-Mouse/Rabbit IgG polymer (Beijing ZSGB Bio-technology Co., Ltd., Beijing, China; Cat. No. PV-6000; Lot No. 2615D0307) for 30 minutes at room temperature and then DAB staining. Between steps, the slides were washed with phosphate-buffered saline (PBS) to remove any unbound primary and secondary antibodies. To validate antibody specificity, the following controls were set: the positive controls consisted of HCC experimental group sections incubated with the primary antibody, where clear and specific SUMO2-positive staining demonstrated the functionality and validity of the antibody under experimental conditions; the negative controls consisted of identical HCC tissue sections in which the primary antibody was replaced with PBS, showing no specific staining and confirming that the staining signal originated from the specific binding of the anti-SUMO2 antibody. All the samples were stained within the same batch to avoid inter-batch variation, and the staining results were independently assessed by two senior pathologists and comprehensively scored using a semi-quantitative scoring system, with a kappa value of $\kappa > 0.8$ ($p < 0.05$) demonstrating a high degree of inter-observer concordance. The literature-referenced scoring criteria for staining intensity were defined as follows: 0 (no staining), 1 (pale yellow), 2 (light brown), and 3 (dark brown). The scoring criteria for the percentage of positive cells were set as: 0 (≤5%), 1 (6%–25%), 2 (26%–50%), 3 (51%–75%), and 4 (≥76%). The final comprehensive IHC score was obtained by multiplying the staining intensity score by the positive cell percentage score, yielding a total score ranging from 0 to 12 [20,21].

This study was approved by the Ethics Committee of the First Affiliated Hospital of Guangxi Medical University (Approval No.: 2020-KY-Guoji-058). Written informed consent was provided by all patients or their legal representatives, and all the experimental procedures were strictly

conducted in adherence to the ethical principles of the Declaration of Helsinki.

2.2 External Proteomic Data Analysis

Given the relatively small sample size of the non-HCC control group in the IHC staining for SUMO2 protein and to minimize potential bias, the SUMO2 proteomic expression data were retrieved from the external Proteomic Data Commons - cProSite database (https://cprosite.ccr.cancer.gov/), including 159 HCC samples and matched control samples, for independent validation and for the calculation of the standardized mean difference (SMD) in combination with the IHC meta-analysis. The raw tandem mass spectrometry (MS/MS) data were processed through standard pipelines, including quality control, peptide identification, and protein quantification. The expression values were log2-transformed and normalized, and the statistical significance was evaluated using the Wilcoxon test ($p < 0.05$). **Supplementary Table 1** presents the processed, log2-transformed and median-normalized SUMO2 protein abundance values retrieved from the cProSite platform.

2.3 Bulk RNA-seq Data Collection, Normalization, and Integration

RNA-seq and gene microarray datasets containing paired HCC and non-HCC liver tissue samples were systematically retrieved from public databases, including The Cancer Genome Atlas (TCGA, https://portal.gdc.cancer.gov/), Gene Expression Omnibus (GEO, https://www.ncbi.nlm.nih.gov/geo/), International Cancer Genome Consortium (ICGC, https://icgc.org/), ArrayExpress (https://www.ebi.ac.uk/arrayexpress/), and Genotype-Tissue Expression (GTEx, https://gtexportal.org/) database. Inclusion criteria: (1) Samples derived from humans; (2) after merging datasets sharing the same gene expression omnibus platform (GPL), the combined dataset must contain both HCC and non-tumor liver tissue controls (individual datasets are permitted to contain only one sample type); (3) Sample size ≥3 per original dataset, and after merging, each platform cohort contained ≥3 HCC samples and ≥3 non-tumor liver tissue control samples. Exclusion criteria: (1) Sample size <3; (2) missing SUMO2 expression data; (3) samples containing metastatic or recurrent HCC. The workflow of the bulk RNA-seq dataset screening is shown in **Supplementary Fig. 1**. The raw expression data from each included platform were preprocessed with standardized procedures based on platform information, including background correction and quantile normalization. Probes were mapped to gene symbols using platform-specific annotation packages (detailed information of the included datasets and sample numbers is provided in **Supplementary Table 2**). Subsequently, the datasets utilizing the same GPL platform were merged, and batch effects were corrected using the ComBat method implemented in the R package sva. To ensure the power of the comprehensive analysis, all the analyses were performed on the merged complete cohort containing both tumor and control samples. A meta-analysis of all genes was conducted using the R package meta v4.18-2 (https://CRAN.R-project.org/package=meta) to calculate the SMD.

Based on the included RNA-seq data, genes consistently meeting the following criteria in ≥9 datasets were defined as SUMO2 co-expressed genes via SMD and Spearman correlation analysis: (1) Positive co-expression: R >0.3, $p < 0.05$; (2) Negative co-expression: R <–0.3, $p < 0.05$. The intersection of SUMO2 positive/negative co-expressed genes with genes having SMD >1 yielded SUMO2 positive and negative co-expressed gene sets (POS-CEGs and NEG-CEGs) that are upregulated in HCC.

2.4 Comprehensive Analysis of SUMO2 at the Single-Cell RNA Sequencing (scRNA-seq) Level

The scRNA-seq dataset GSE149614, comprising 10 primary HCC samples and 8 non-HCC liver tissue samples, was retrieved from the GEO database. The raw count matrices were processed and analyzed using theR package Seurat v4.4.0 (Satija Lab at NYGC, New York, NY, USA). A total of 63,101 cells were initially obtained. The quality control (QC) criteria were applied as follows: (1) cells with fewer than 200 detected genes were excluded; (2) cells with more than 8000 detected genes were excluded (to remove potential doublets or technical artifacts); (3) cells with mitochondrial gene content >25% were excluded. After QC, 58,984 high-quality cells were retained for subsequent analyses. Normalization was performed using the LogNormalize method with a scale factor of 10,000 per cell. A total of 2000 highly variable genes were identified (using the vst method). Principal component analysis (PCA) was conducted, and the top 23 principal components were selected for downstream dimensionality reduction. The batch effects across samples were corrected using the Harmony algorithm. Unsupervised clustering was performed using a shared nearest neighbor (SNN) graph with a resolution of 0.1 (FindClusters function (part of Seurat v4.4.0, Satija Lab at NYGC, New York, NY, USA)), yielding multiple transcriptionally distinct cell clusters. Uniform manifold approximation and projection (UMAP) was employed for visualization. To further remove remaining doublets, we applied DoubletFinder v3.0 (https://github.com/chris-mcginnis-ucsf/DoubletFinder) with the parameter pN set to 0.25, and a total of 3478 cells were removed. Ultimately, 55,506 cells were retained for subsequent cell annotation, with a balanced contribution across samples and no apparent bias. The cell types were annotated manually based on the expression of the canonical marker genes from published literature [22] and adjusted according to the actual data characteristics, including T/NK cells (CD3D, CD3E, NKG7), B cells (CD79A, JCHAIN, MZB1), myeloid cells (LYZ, CD68, CD14), endothelial cells (CDH5, CLDN5, VWF), fibroblasts (COL1A1, ACTA2), and hepatocytes

(APOA1, APOC3). To identify malignant cell populations, the scRNA-seq data from HCC samples alone were extracted, and the copy number variations (CNV) were inferred using the inferCNVpy tool (https://github.com/icbi-lab/infercnvpy) [23], with T/NK and B cells as references. The cells with a CNV score >0.01 and significantly higher CNV signals than the background were defined as malignant cells. Based on this, these cells were grouped according to SUMO2 expression levels and further divided into high and low expression subpopulations.

To systematically decipher the biological functions associated with differential SUMO2 expression, multiple tools were integrated for multi-dimensional analyses, including CytoTRACE2 (v1.1.0) [24] for cell developmental potential, monocle3 (v1.3.4) for pseudotime differentiation trajectory, scTenifoldKnk (v1.0.2) [25] for regulatory networks of perturbed genes after gene knockout, CellChat (v1.6.1) [26] for cell–cell communication networks and signaling pathway activity, mebocost (v1.0.4) [27] for metabolite-mediated cell interactions, scMetabolism (v0.2.1) [28] for cell-type-specific metabolic scoring, scFEA (v1.1.2) [29] for metabolite flux transformation, and scRank (v1.0.0) [30] for predicting the sensitivity of different cell subpopulations to potential therapeutic drugs.

2.5 Spatial Expression and Localization Analysis of SUMO2 in Spatial Transcriptomics (ST)

The ST data used were obtained from the GEO database (accession number: GSE245908; sample ID: GSM7850823). The gene expression matrix of the ST data was constructed using the Seurat package in R, and the raw count data were normalized and variance-stabilized using the SCTransform method. Based on the cell type annotation results from the aforementioned scRNA-seq analysis, the cellular composition of each spatial spot was inferred via reference-based deconvolution (RCTD). Subsequently, the SpaCET R package was used to estimate the relative abundance of malignant tumor cells at each spatial location [31]. Additionally, the spatial expression pattern of SUMO2 in liver tissue sections was visualized, and regions were divided into high and low SUMO2 expression areas based on the median SUMO2 expression level. Furthermore, the scMetabolism R package was employed to calculate metabolic pathway activity scores for these two types of regions, aiming to explore the potential association between differential SUMO2 expression and local metabolic states.

2.6 SUMO2 Expression and CRISPR Knockout in HCC Cell Lines

The data on SUMO2 mRNA expression in HCC cell lines and CRISPR-Cas9 knockout screening were obtained from the DepMap Portal database (https://depmap.org/portal/; version 24Q3). The Chronos score was used to evaluate the effect of SUMO2 knockout on cell proliferation. Chronos is a Bayesian framework-based algorithm that eliminates false-positive signals caused by copy number amplification and corrects for experimental noise. A negative Chronos score (<0) indicates that cell growth is inhibited following gene knockout [32]. All the cell line data in the DepMap platform undergo rigorous quality control procedures: The cell line identity is confirmed by short tandem repeat (STR) analysis, and mycoplasma contamination is routinely tested to ensure culture purity; lineage validation, mutation status, and transcriptomic consistency are cross-validated against the cancer cell line encyclopedia (CCLE) public reference dataset (https://sites.broadinstitute.org/ccle) to prevent cell line misidentification or cross-contamination. In addition, DepMap applies standardized data normalization and batch effect correction (including the removal of platform-specific differences and experimental batch effects) to ensure reproducibility and comparability across experimental replicates and cell line panels. These integrated quality control steps guarantee the reliability and biological validity of the SUMO2 dependency data used in this study [33].

2.7 Enrichment Analysis

First, based on the aforementioned SUMO2-co-expressed gene sets upregulated in HCC, enrichment analysis was performed using the clusterProfiler package v4.8.2 (YuLab-SMU, Guangzhou, Guangdong, China) with data from the Gene Ontology (GO) and Kyoto Encyclopedia of Genes and Genomes (KEGG) databases. Additionally, using tumor samples from the combined TCGA-GTEx dataset, the HCC samples were stratified into high and low SUMO2 expression groups according to the median expression level. Differential expression analysis was performed with the edgeR package: The lowly expressed genes were filtered using filterByExpr function (part of edgeR package, WEHI, Melbourne, Victoria, Australia), TMM normalization was applied, a generalized linear model was fitted, and the high versus low expression groups were compared using a likelihood ratio test, yielding $\log_2$ fold changes (logFC) for all genes. Genes were ranked by logFC in descending order and used as input for gene set enrichment analysis. The human hallmark gene set (h.all.v2025.1.Hs.symbols.gmt) was retrieved from the MSigDB database, and GSEA was conducted using the GSEA function of the clusterProfiler package with 1000 permutations, reporting the normalized enrichment score (NES). Finally, the GeneMANIA database (https://genemania.org/) was used to further predict the potential biological functions of SUMO2-interacting gene sets.

2.8 Immune Infiltration Analysis

Using the TCGA-GTEx combined dataset as the training cohort, the CIBERSORTx algorithm was employed to quantify the proportions of 22 immune cell subsets in the

high and low SUMO2 expression groups. Further comparisons of the intergroup differences and correlations with SUMO2 expression levels were conducted.

2.9 Clinical Parameter Analysis

The biomarker exploration and systematic tool (BEST) was used to systematically integrate the differences between high and low SUMO2 expression groups in terms of survival outcomes (Log-rank test), clinicopathological characteristics (*t*-test, ANOVA, and Kruskal-Wallis test), and genomic mutation profiles, enabling multi-dimensional biomarker exploration [34].

2.10 Drug Sensitivity Prediction and In Silico Docking Analysis

Based on the HiPlot cloud analysis platform (https://rookieutopia.hiplot.com.cn/app_direct/BEST/#PageHomeAnalysisModuleSelection), the half-maximal inhibitory concentration (IC50) data from three major drug sensitivity databases—Genomics of Drug Sensitivity in Cancer (GDSC), Cancer Therapeutics Response Portal (CTRP), and Profiling Relative Inhibition Simultaneously in Mixtures (PRISM)—were used to calculate the correlation coefficients between drug sensitivity and SUMO2 expression in each transcriptomic dataset. The average correlation coefficient across the three databases was taken as a composite score; a negative coefficient indicates that the drug is more sensitive to samples with high SUMO2 expression. The Benjamini-Hochberg method was applied to correct the p-values for each drug, and candidates with a false discovery rate (FDR) <0.05 were identified as significant. These candidates were then ranked by the average correlation coefficient to determine the drugs with the most significant correlation coefficients for further *in silico* evaluation.

To perform computational docking prediction between the candidate drugs and the SUMO2 protein, the high-resolution three-dimensional structure of SUMO2 (PDB ID: 7P99) was downloaded from the Protein Data Bank (PDB; https://www.rcsb.org/). Meanwhile, the three-dimensional chemical structures of the candidate small molecules were obtained from the PubChem database (https://pubchem.ncbi.nlm.nih.gov/): BRD-K71781559 (CID: 246676), IU1 (CID: 675434), Aminopentamide (CID: 22565), Zuclopenthixol (CID: 5311507), Sepantronium bromide (CID: 11178236), and Dasatinib (CID: 3062316). Subsequently, blind docking simulations were performed using the CB-Dock2 online molecular docking server (http://clab.labshare.cn/cb-dock2/). The CB-Dock2 docking procedure was as follows: (1) the protein and small-molecule structure files were input and subjected to quality checks; (2) the structural data were automatically preprocessed, including the repair of missing atoms and hydrogen atoms and the removal of water molecules and other heteroatoms; (3) curvature-based cavity detection was used to identify the binding pockets on the protein surface, and molecular docking was scored with AutoDock Vina, searching the top five most-favorable binding pockets and estimating their spatial parameters; (4) the results were comprehensively processed and visualized. In this study, a Vina score ≤ -5.0 kcal/mol was adopted as a threshold for identifying docking poses with relatively favorable predicted binding energies. The conformation with the lowest predicted binding free energy was selected as the optimal docking mode for each candidate drug. It should be noted that these docking results are purely computational predictions and do not substitute for experimental validation; further biochemical assays, such as cellular binding or functional competition studies, would be required to confirm any actual physical interaction or biological relevance.

2.11 Statistical Analysis

Except for the statistical methods specifically mentioned above, all the statistical analyses and algorithms in this study were implemented using R v4.3.1 (R Foundation for Statistical Computing, Vienna, Austria)and Python v3.10 (Python Software Foundation, Wilmington, DE, USA). The high and low SUMO2 expression groups were divided based on the median of the normalized expression levels—if the median was zero, the samples with expression >0 were assigned to the high expression group. After merging the datasets on the same GPL platform and correcting batch effects with ComBat, the I^2 statistic was calculated to assess the heterogeneity of each gene in the meta-analysis. For pooled datasets with low heterogeneity (I^2 <50%), a fixed-effects model was used to calculate the SMD; for pooled datasets with high heterogeneity (I^2 ≥50%), a random-effects model was applied instead. The 95% confidence interval (CI) of SMD: if the 95% CI did not include zero, the between-group difference was considered statistically significant; if it included zero, the difference was not significant. A p value > 0.05 in the Begg and Egger tests indicated no significant publication bias in the SMD results across cross-platform analyses. For multiple hypothesis testing, the Benjamini–Hochberg method was uniformly applied to control the false discovery rate (FDR) in enrichment analyses (GO/KEGG, GSEA), immune infiltration, drug sensitivity screening, and mutation analyses (including gene mutation frequency and mutation burden). For GSEA, FDR <0.25 was considered significant as recommended; for all other analyses, FDR <0.05 was applied. For multiple group comparisons of clinicopathological parameters, Bonferroni correction was used (k comparisons, corrected $\alpha = 0.05/k$), with a corrected $p < 0.05$ considered significant. The pROC package was used to generate receiver operating characteristic (ROC) curves, and STATA 16.0 (StataCorp LLC, College Station, TX, USA) was used to construct summary ROC (sROC) curves. The area under the curve (AUC) was used to evaluate the SUMO2 expression levels, with an AUC value closer to 1 reflecting a more

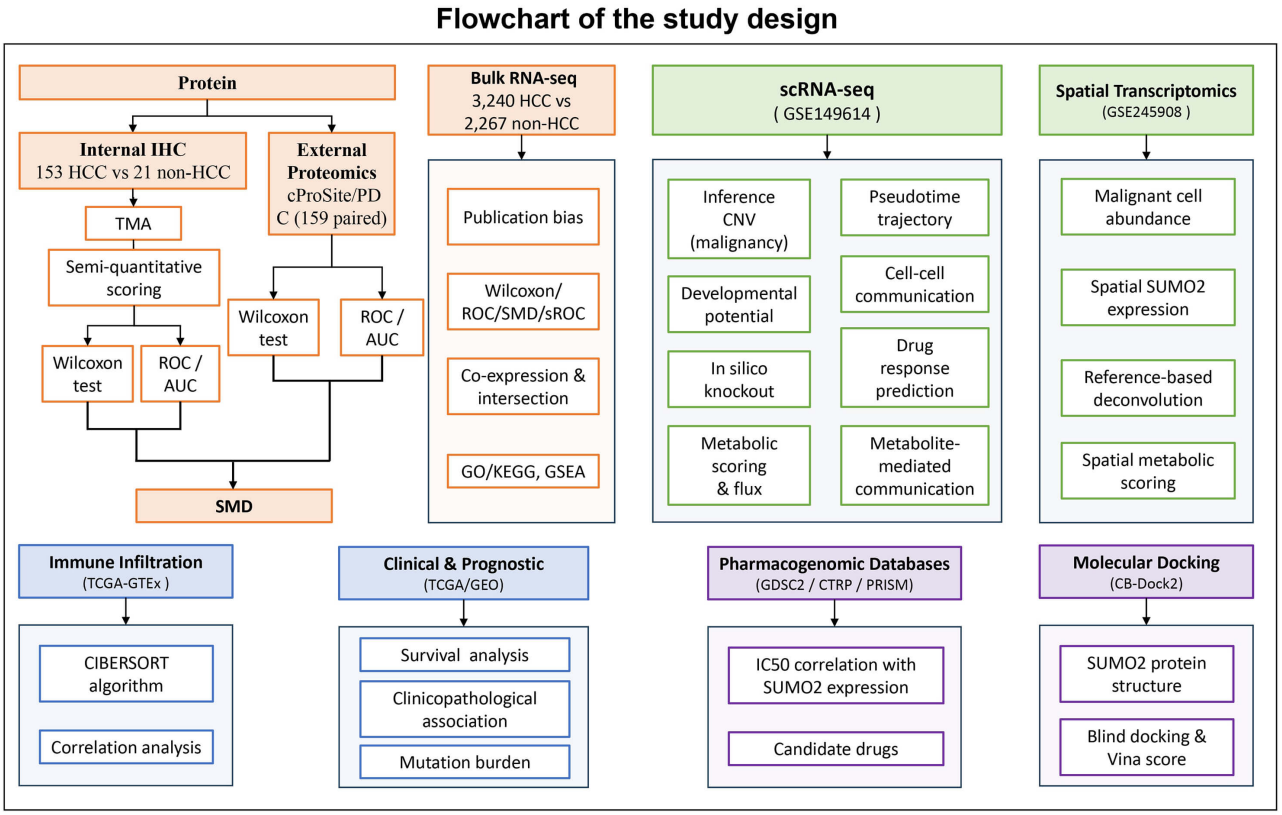

Fig. 1. Flowchart of the present study design (Microsoft Corporation, Redmond, WA, USA). IHC, immunohistochemistry; HCC, hepatocellular carcinoma; TMA, tissue microarray; PDC, Proteomic Data Commons; CNV, copy number variations; KEGG, Kyoto Encyclopedia of Genes and Genomes; GO, Gene Ontology; GSEA, Gene Set Enrichment Analysis; CTRP, Cancer Therapeutics Response Portal; GDSC, Genomics of Drug Sensitivity in Cancer; SUMO2, small ubiquitin-like modifier 2.

significant high-expression efficacy [35]. Additionally, a $p < 0.05$ was considered statistically significant unless otherwise specified. The study design flowchart is presented in Fig. 1.

3. Results

3.1 SUMO2 Protein Is Overexpressed in HCC Specimens

In the in-house IHC experiment (153 HCC vs. 21 non-HCC), SUMO2 immunostaining in HCC tissues was predominantly localized to tumor cell nuclei, with weak to moderate diffuse or focal strong positivity in the cytoplasm, and the staining intensity was markedly higher than in non-HCC tissues (Fig. 2A,B). This expression exhibited a significant differential diagnostic value with high efficacy ($p < 0.05$; AUC = 0.995; Fig. 2C,D). Given the small sample size of the non-HCC control group, which may lead to an overestimation of the diagnostic AUC of IHC, an independent analysis was performed using the external cProSite proteomic database to avoid potential bias from the single-center small control cohort. In 159 matched HCC and non-HCC samples, the SUMO2 protein levels were also significantly upregulated in HCC ($p < 0.05$; AUC = 0.827; Fig. 2E,F). Further combined SMD analysis of the internal and external data, encompassing a total of 312 HCC and 180 non-HCC samples, demonstrated that SUMO2 protein expression was consistently and significantly elevated in HCC (SMD = 2.06; 95% CI: 0.42–3.69; Fig. 2G), thereby confirming the robustness of SUMO2 upregulation irrespective of single-cohort sample imbalance.

3.2 SUMO2 mRNA Is Significantly Upregulated in HCC

To comprehensively assess the transcriptional landscape of SUMO2 in HCC, the bulk RNA sequencing data from 34 independent platforms were integrated. The comparative analysis with non-tumor liver tissues revealed that SUMO2 exhibited significantly elevated expression in HCC samples across 8 platforms, with both statistical significance ($p < 0.05$) and high diagnostic discriminability (AUC >0.7; **Supplementary Fig. 2**; **Supplementary Fig. 3**). A meta-analysis was subsequently performed by aggregating all the eligible datasets, encompassing 3240 HCC specimens and 2267 non-HCC controls. The pooled estimate demonstrated a consistent and significant upregulation of SUMO2 mRNA in HCC (SMD >0; 95% CI: 0.39–0.90; Fig. 3A), accompanied by robust discriminatory performance (sROC = 0.80; Fig. 3B). The assessment of publi-

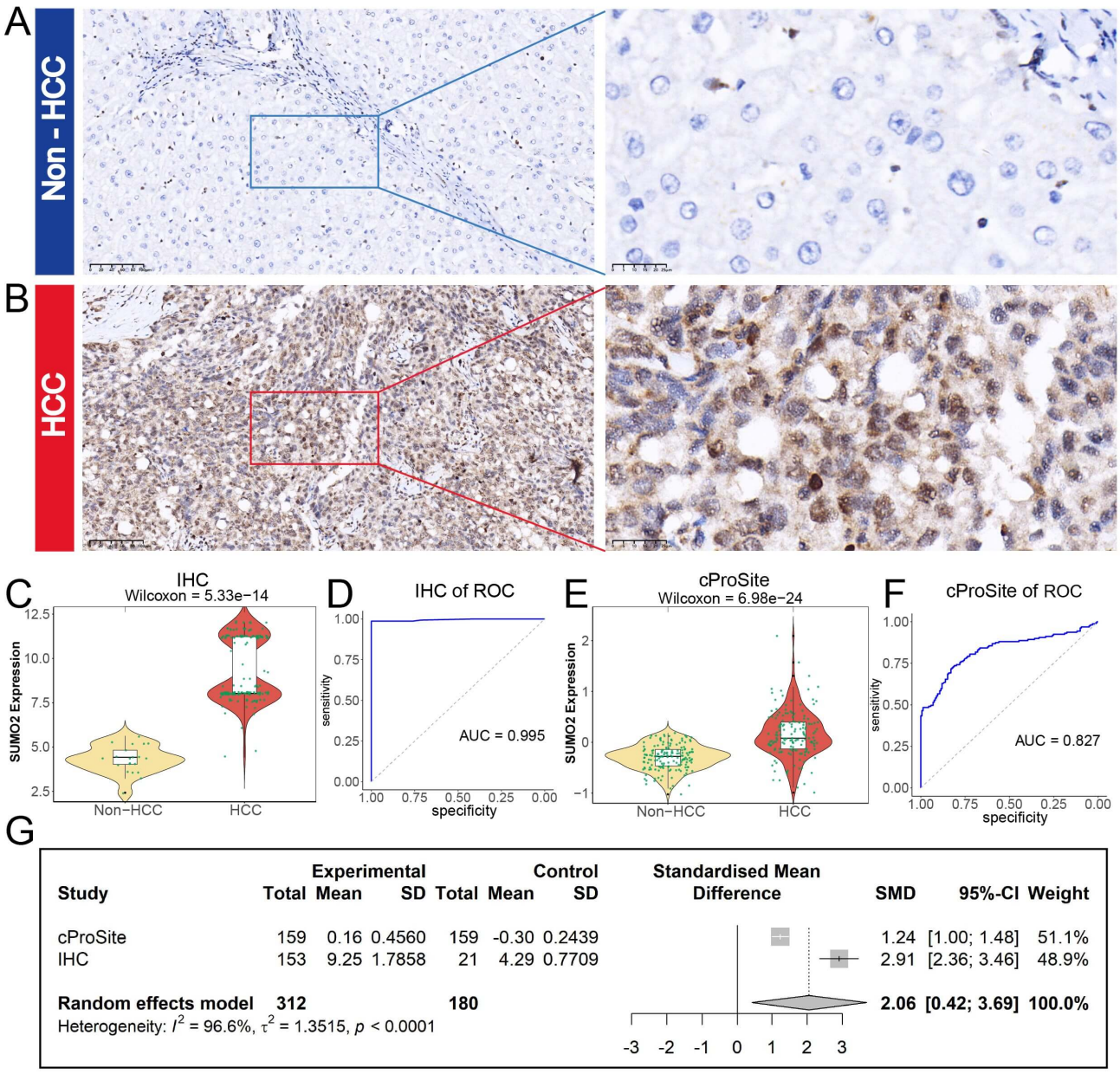

Fig. 2. Analysis of SUMO2 protein expression. (A) Microscopic images of IHC staining for SUMO2 protein in non-HCC tissues, scale bars: 100 µm and 25 µm (enlarged images); (B) Microscopic images of IHC staining for SUMO2 protein in HCC tissues, scale bars: 100 µm and 25 µm (enlarged images); (C) Intergroup Wilcoxon test analysis of IHC scores; (D) ROC curve analysis of IHC experiments; (E) Intergroup Wilcoxon test analysis of cProSite proteomic data; (F) ROC curve analysis of cProSite proteomic data; (G) Comprehensive SMD analysis of summarized SUMO2 protein expression data.

cation bias using Egger's and Begg's tests indicated no significant asymmetry ($p > 0.05$; Fig. 3C,D), thus supporting the reliability and generalizability of the findings.

3.3 SUMO2 Is Widely Expressed in Malignant Hepatocytes

The scRNA-seq analysis was employed to delineate the cellular distribution of SUMO2 within HCC. A total of 10 HCC specimens and 8 non-HCC controls were analyzed, resulting in the identification of 10 distinct clusters (Fig. 4A,B). Based on the expression profiles of canonical marker genes, these clusters were annotated as B cells, endothelial cells, fibroblasts, hepatocytes, myeloid cells, and T/NK cell populations (Fig. 4C,D). The examination of SUMO2 expression revealed its enrichment predominantly within hepatocyte, myeloid, and T/NK cell populations, as illustrated by the UMAP plots and violin plots (Fig. 4E,F). To further validate the malignant status of the hepatocyte cluster, CNV inference was performed exclusively

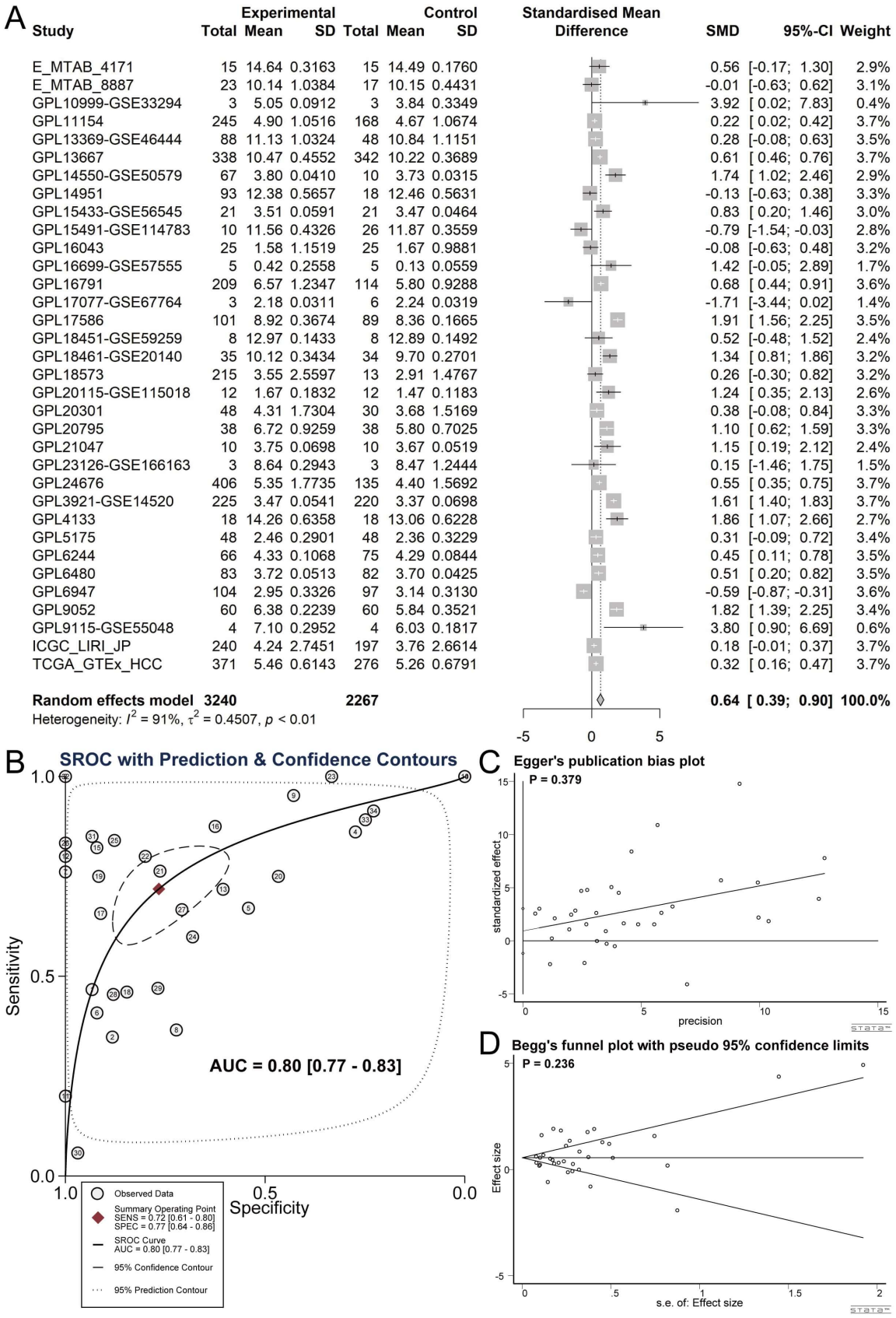

Fig. 3. Comprehensive analysis of SUMO2 expression at the mRNA level. (A) Forest plot of the overall SMD for SUMO2 expression; (B) sROC analysis; (C) Egger's test; (D) Begg's test.

on HCC samples using T/NK and B cells as reference populations. This analysis demonstrated significant chromosomal amplifications and deletions within the hepatocyte population, confirming their identity as malignant hepatocytes (Fig. 4G–I), thereby validating the accuracy of cell type annotations. Notably, SUMO2 exhibited widespread and significantly elevated expression levels, specifically within the malignant hepatocytes of HCC samples (Fig. 4J).

3.4 SUMO2 Is Highly Expressed in Malignant Tumor Regions

To further elucidate the spatial distribution of SUMO2 within tumor regions, scRNA-seq data were integrated with ST for deconvolution analysis. This approach revealed a pronounced presence of hepatocytes within the tumor areas (**Supplementary Fig. 4A**). The subsequent analysis involving malignant tumor cell scoring and SUMO2 expression demonstrated that SUMO2 is highly expressed within the spatial regions occupied by malignant tumor cells (**Supplementary Fig. 4B–E**). These findings suggest that SUMO2 plays a critical role in the malignant transformation and progression of hepatocytes within HCC tumors.

3.5 Public CRISPR Screening Data Suggest That SUMO2 Knockout Inhibits Proliferation of HCC Cell Lines

The data from public functional genomics resources support the significant expression of SUMO2 in 22 HCC cell lines (such as SNU398, JHH4, and JHH1; **Supplementary Fig. 5A**). Concurrently, the external CRISPR/Cas9-mediated data also demonstrated that SUMO2 knockout significantly inhibited the proliferative capacity of 19 of these cell lines (such as SNU182, JHH6, and JHH7; **Supplementary Fig. 5B**).

3.6 SUMO2 Is Significantly Enriched in Metabolism-Related Pathways

Further functional enrichment analysis of bulk RNA-seq data, focusing on the gene sets co-expressed with SUMO2 and highly expressed in HCC, elucidated its molecular mechanisms (**Supplementary Fig. 6**). The intersection analysis of the SUMO2 positively co-expressed genes (SUMO2 POS-CEGs) (**Supplementary Fig. 6A**) demonstrated that among the 3430 unique genes highly upregulated in HCC (SMD >1), 240 significant genes were obtained from the intersection with POS-CEGs positively correlated with SUMO2 (R >0.3), while 39 genes were obtained from the intersection with NEG-CEGs negatively correlated with SUMO2 (R <–0.3) (**Supplementary Fig. 6B**). Moreover, the GO and KEGG enrichment analysis of the positively correlated genes revealed that these genes were significantly enriched in core mechanisms such as cell cycle regulation, DNA replication and repair, and chromosome segregation. They were also involved in molecular mechanisms related to protein kinase activity, ubiquitination modification, and microtubule binding. Furthermore, enrichment was found in glycolysis/oxidative phosphorylation-related metabolic reprogramming pathways such as the tricarboxylic acid (TCA) cycle, pentose phosphate pathway, and glycerophospholipid metabolism, as well as immune-associated processes such as antigen presentation and glutathione metabolism (**Supplementary Fig. 6C,D**). The GO and KEGG enrichment analyses of the negatively correlated genes indicated that these genes were focused on the pathways related to lipid metabolism, oxidoreductase activity, and hormone signaling (**Supplementary Fig. 6E,F**).

The GeneMANIA analysis of the gene interaction networks showed that the glycolytic process, ATP metabolic process, carbohydrate catabolic process, and pyruvate metabolic process are significant key pathways interacting with the SUMO2 gene (**Supplementary Fig. 7A**).

The GSEA analysis based on the Hallmark gene sets from the MSigDB database, using SUMO2 single-gene grouping, revealed significant enrichment in metabolism-related pathways such as bile acid metabolism, fatty acid metabolism and adipogenesis, DNA repair, mitotic spindle and G2/M checkpoint, interferon gamma response, KRAS signaling, and MYC target genes. This suggests that SUMO2 is highly associated with functions related to metabolism, cell cycle progression, and immune response, thereby influencing the development and progression of HCC (**Supplementary Fig. 7B**).

3.7 scRNA-seq Reveals the Key Regulatory Role of Metabolism in the Developmental Trajectory of Malignant Hepatocytes

cytoTRACE2 was employed to analyze the developmental differentiation potential of cells in the scRNA-seq HCC samples. It was found that hepatocytes possessed high differentiation potential (Fig. 5A–D). Subsequently, pseudotime trajectory analysis was performed specifically on the hepatocyte cluster, which revealed that SUMO2 expression initially decreased from early to mid-pseudotime, followed by an increase in late pseudotime, and then reached its highest peak (Fig. 5E–I). Furthermore, GO enrichment analysis was conducted on differentially expressed genes across various developmental trajectory branches, finding that the developmental trajectory was composed of multiple branches with distinct functions corresponding to specific metabolic, proliferative, or immune processes: Branch C5 was enriched in steroid and cholesterol metabolism as well as peptide antigen processing and presentation; branch C4 was highly enriched in mitosis-related processes, including chromosome segregation, spindle organization, and nuclear division; branch C3 encompassed the anabolism and catabolism of the intracellular small molecules, including organic acids, carboxylic acids, amino acids, fatty acids, and steroids; branch C2 was enriched in fatty acid metabolism, cellular detoxification, and MHC class II protein complex assembly; and branch C1 was significantly

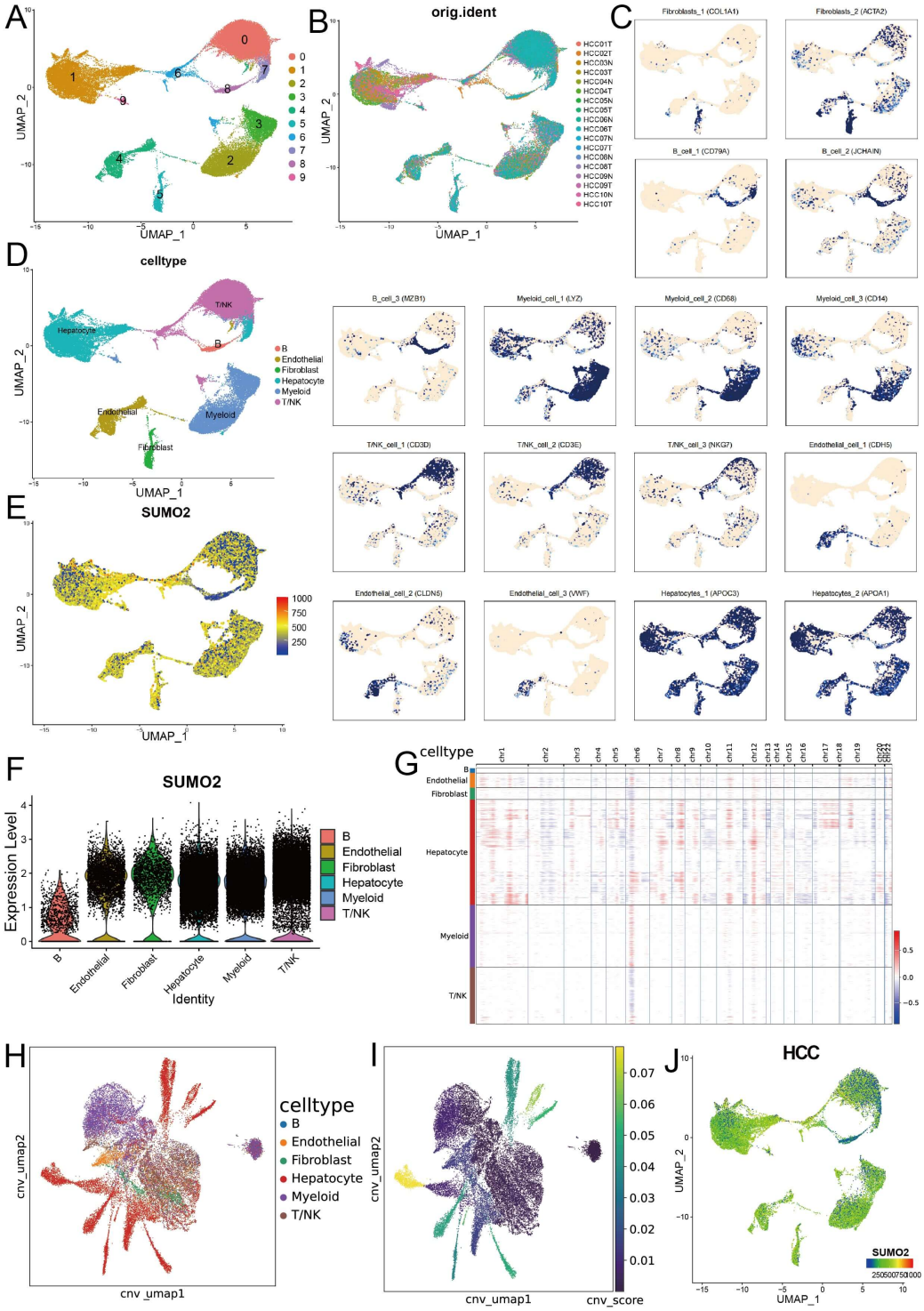

Fig. 4. Expression analysis of SUMO2 at the scRNA-seq level. (A) UMAP plot showing scRNA-seq clustering of cells from HCC and non-HCC samples; (B) UMAP plot depicting sample-specific clustering; (C) UMAP plot illustrating the expression of marker genes across different cell types; (D) UMAP plot with annotation for six cell types: B cells, endothelial cells, fibroblasts, hepatocytes, myeloid cells, and T/NK cells; (E) UMAP plot displaying SUMO2 expression levels across various cell types; (F) Violin plots showing SUMO2 expression levels in different cell types; (G) Heatmap representing CNV scores in HCC samples; (H) UMAP projection of CNV scores across cell types; (I) Distribution of CNV scores. (J) SUMO2 expression distribution in HCC samples. UMAP, uniform manifold approximation and projection; CNV, copy number variations.

enriched in ribosome biogenesis, cytoplasmic translation, and regulation of DNA synthesis (Fig. 5J).

3.8 scRNA-seq Analysis Predicts the Regulation of Metabolic Functions by Perturbed Gene Networks Upon Virtual Knockout of SUMO2

Based on the scRNA-seq data, an *in silico* knockout simulation of the SUMO2 gene was performed in malignant hepatocytes. The significantly differentially regulated genes were screened, and the KO-SUMO2 perturbation results were visualized as a volcano plot ($|Z| > 2$, $p < 0.05$; Fig. 6A).

The functional enrichment analysis of the positively responsive differentially expressed genes (a total of 123 genes) with $Z \geq 2$ and $p < 0.05$ revealed significant KEGG pathway enrichment in the biological processes centered on metabolic reprogramming, including glycolysis and pyruvate metabolism. Concurrently, the immune and inflammation-related pathways (such as HIF-1 and IL-17 signaling pathways) were also significantly activated. Furthermore, the pathways involved in cell motility and structural dynamics regulation, such as motor proteins and cell adhesion molecules, were implicated (Fig. 6B). The GO analysis further corroborated the aforementioned three major themes: metabolic stress response (e.g., carbohydrate catabolic process, oxidoreductase activity, Ras protein signal transduction); immune and inflammatory response (including cytokine signaling, humoral immune response, and complement activation); and regulation of cell motility and adhesion (e.g., cadherin binding and cell-cell adhesion mediator activity) (Fig. 6C).

On the other hand, the enrichment analysis of the differentially expressed genes with negative effects (a total of 258 genes) meeting $Z \leq -2$ and $p < 0.05$ revealed that the KEGG pathways were primarily enriched in immunodeficiency, metabolic abnormalities, phagocytosis and autophagy functions, and other metabolic pathways (Fig. 6D). The GO analysis showed significant enrichment in T-cell activation, regulation of T-cell differentiation, epigenetic regulation mediated by transcriptional repressor complexes (e.g., Sin3/HDAC complex), and processes related to cytoskeleton organization and membrane trafficking (Fig. 6E). However, this analysis is solely computational, and the results should be regarded as hypotheses awaiting experimental validation.

3.9 A SUMO2-High Hepatocyte Subpopulation Enhances MIF Signaling and Metabolite-Mediated Cell–Cell Communication

To dissect the functional implications of SUMO2 heterogeneity within malignant hepatocytes, CellChat-mediated intercellular communication analysis was performed by comparing the SUMO2-high and SUMO2-low subpopulations derived from malignant hepatocytes. The SUMO2-low group exhibited markedly reduced interaction strength and fewer ligand–receptor pairs with endothelial and myeloid cells compared to the SUMO2-high group (Fig. 7A–C). Among the differentially active signaling pathways, the MIF–(CD74–CXCR4)/(CD74–CD44) axis emerged as the most significantly enriched in the SUMO2-high malignant hepatocyte subpopulation (Fig. 7D), prompting a focused investigation of this pathway. Notably, the SUMO2-high malignant hepatocytes displayed substantially stronger communication via the MIF signaling pathway with both T/NK and myeloid cells (Fig. 7E). Further decomposition of the incoming and outgoing signaling roles demonstrated that the SUMO2-high malignant hepatocytes contributed more prominently as "sender" and "influencer" cells in the MIF pathway than their SUMO2-low counterparts (Fig. 7F,G). At the transcriptional level, the key components of the MIF–(CD74–CXCR4) axis were significantly upregulated in the SUMO2-high hepatocyte subpopulation (Fig. 7H). A comprehensive mapping of the global communication landscape further identified additional signaling pathways—such as MK, PARs, and VISFATIN—as major contributors to the differential intercellular crosstalk mediated by the SUMO2-high versus SUMO2-low malignant hepatocytes (Fig. 7I). Collectively, these findings indicate that elevated SUMO2 expression endows a subset of malignant hepatocytes with an enhanced capacity to orchestrate tumor microenvironmental interactions, particularly through the potentiation of MIF-driven signaling networks. Collectively, based on the preliminary computational inferences, the malignant hepatocyte subpopulation with high SUMO2 expression may enhance the signaling network of interactions with the microenvironment through the MIF signaling pathway.

To further infer metabolite-mediated intercellular communication, the MEBOCOST-based analysis revealed that the SUMO2-high hepatocyte subpopulation exhibited a greater number of metabolite-driven sender and receiver communication events compared to the SUMO2-low group, positioning it as a dominant contributor to metabolic crosstalk within the tumor microenvironment (Fig. 8A–C). Notably, the interactions involving hepatocytes (both SUMO2-high and SUMO2-low) and myeloid cells—as either senders or receivers—were prominently enriched for signaling mediated by iron-related metabolites and their associated sensors, particularly TFR2 and SLC40A1 (Fig. 8D,E). Of particular significance, the metabolite D-glucose and the iron-related sensor TFR2 showed markedly elevated levels in the SUMO2-high malignant hepatocyte population (Fig. 8F,G), suggesting the preliminary predictive potential of the SUMO2-high hepatocyte subpopulation in enhancing glucose- and iron-related metabolic communication networks in HCC.

3.10 Joint Validation at scRNA-seq and ST Levels Reveals Key Processes of SUMO2-Affected Metabolic Pathways

Utilizing the data of SUMO2-high and SUMO2-low hepatocyte groups identified by scRNA-seq and

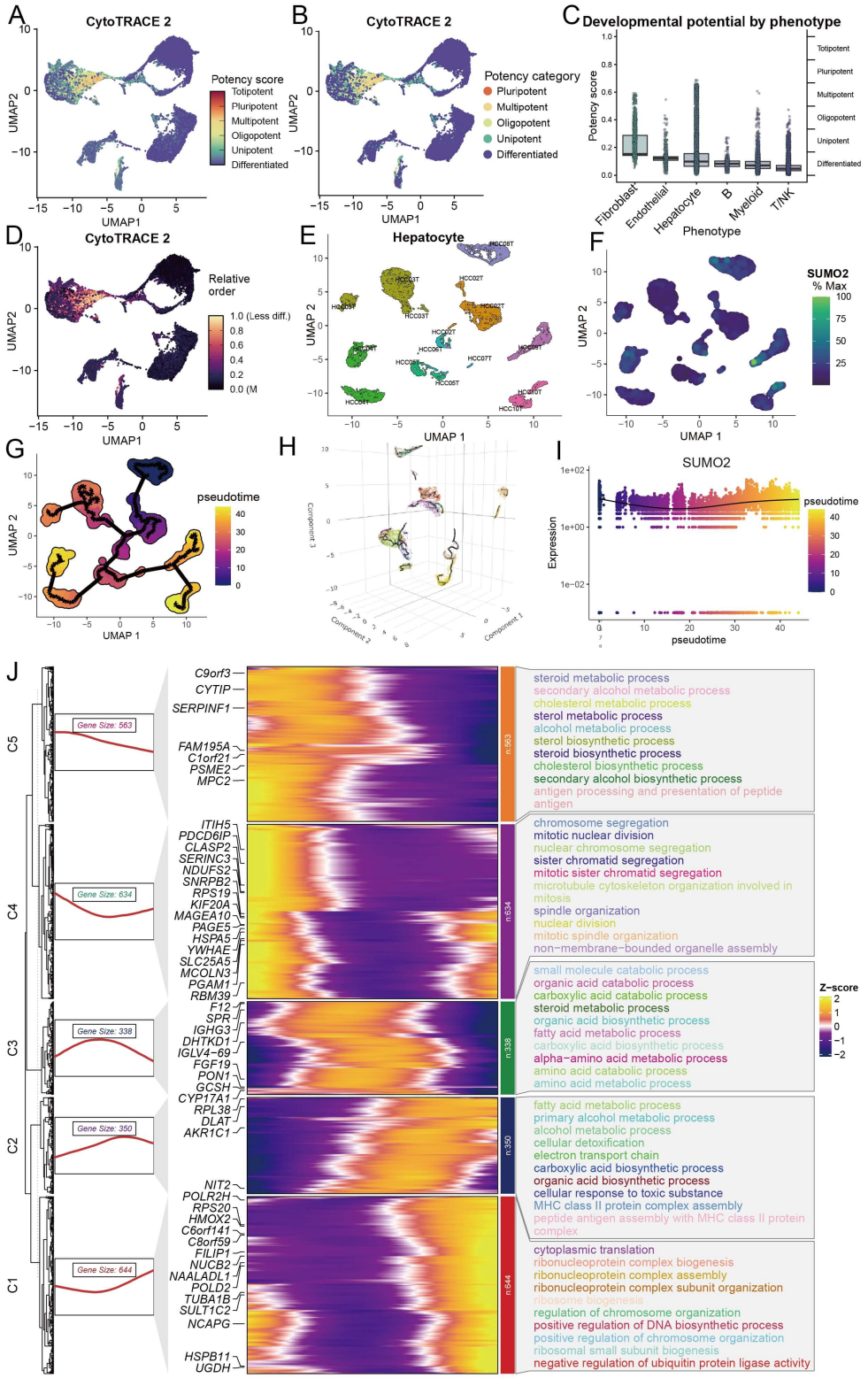

Fig. 5. Developmental potential and pseudotime trajectory analysis of malignant hepatocytes. (A,B) Developmental potential distribution plots across all cell populations (CytoTRACE score); (C) Box plot comparing the developmental potential of different cell phenotypes; (D) Relative order heatmap; (E) UMAP distribution plot of extracted hepatocyte samples; (F) UMAP expression distribution plot of SUMO2 in hepatocytes; (G) 2D projection of inferred cell developmental trajectory based on pseudotime; (H) 3D projection of inferred cell developmental trajectory based on pseudotime; (I) Trend of SUMO2 expression along the pseudotime axis; (J) Differential gene expression characteristics and functional enrichment analysis of each developmental branch (C1–C5).

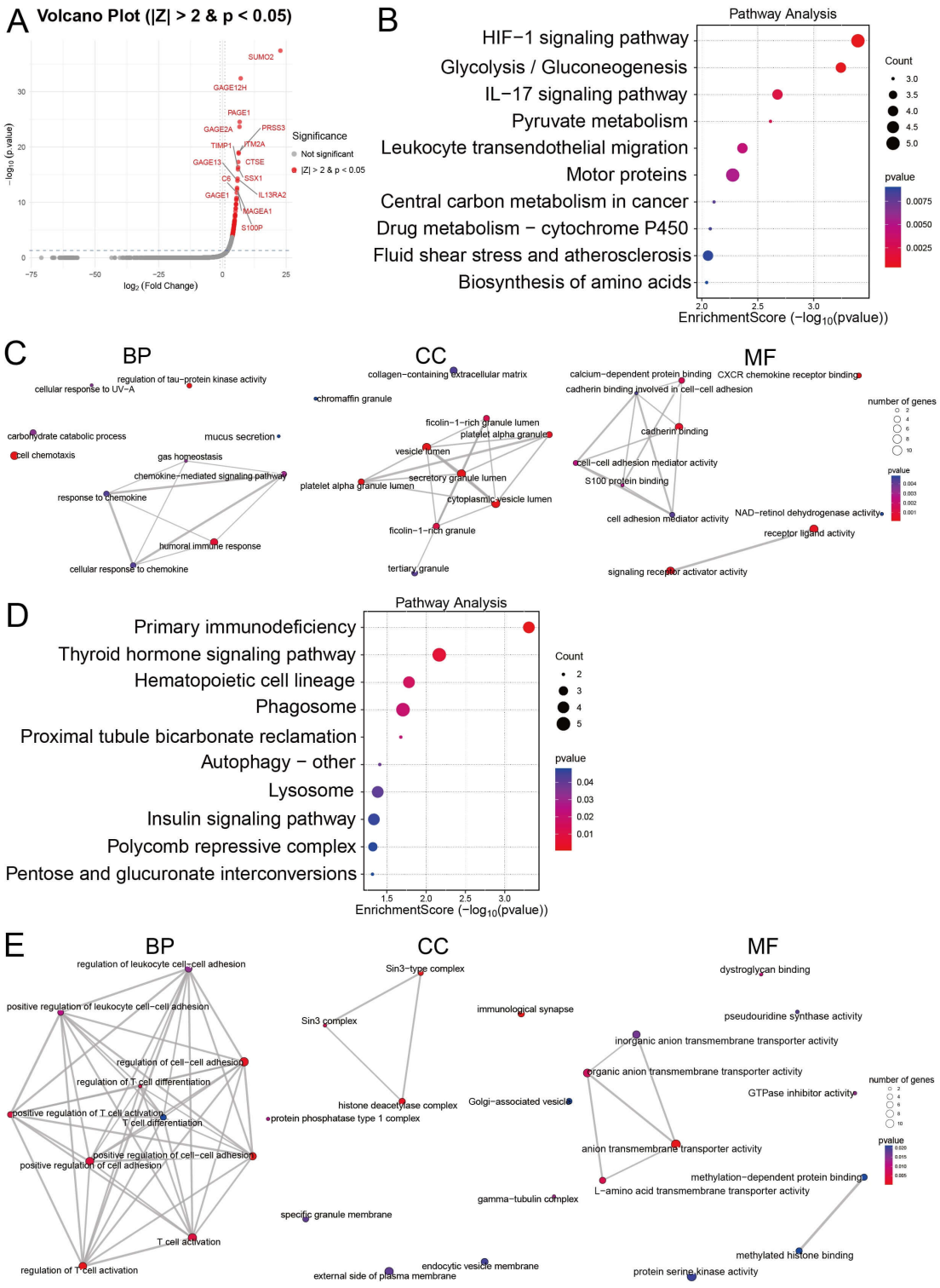

Fig. 6. Analysis of simulated SUMO2 gene knockout in malignant hepatocytes (scTenifoldKnk). (A) Volcano plot of genes significantly perturbed by KO-SUMO2; (B) KEGG enrichment analysis of positively perturbed genes; (C) GO enrichment analysis of positively perturbed genes; (D) KEGG enrichment analysis of negatively perturbed genes; (E) GO enrichment analysis of negatively perturbed genes. BP, Biological Process; CC, Cellular Component; MF, Molecular Function; HIF-1, Hypoxia-Inducible Factor-1.

ST, the computational prediction of metabolic scores via scMetabolism showed that the SUMO2-high group in scRNA-seq was enriched in metabolism-related pathways such as Glycolysis/Gluconeogenesis (Fig. 9A). The SUMO2-high group in ST also showed high consistency with the scRNA-seq results, including signifi-

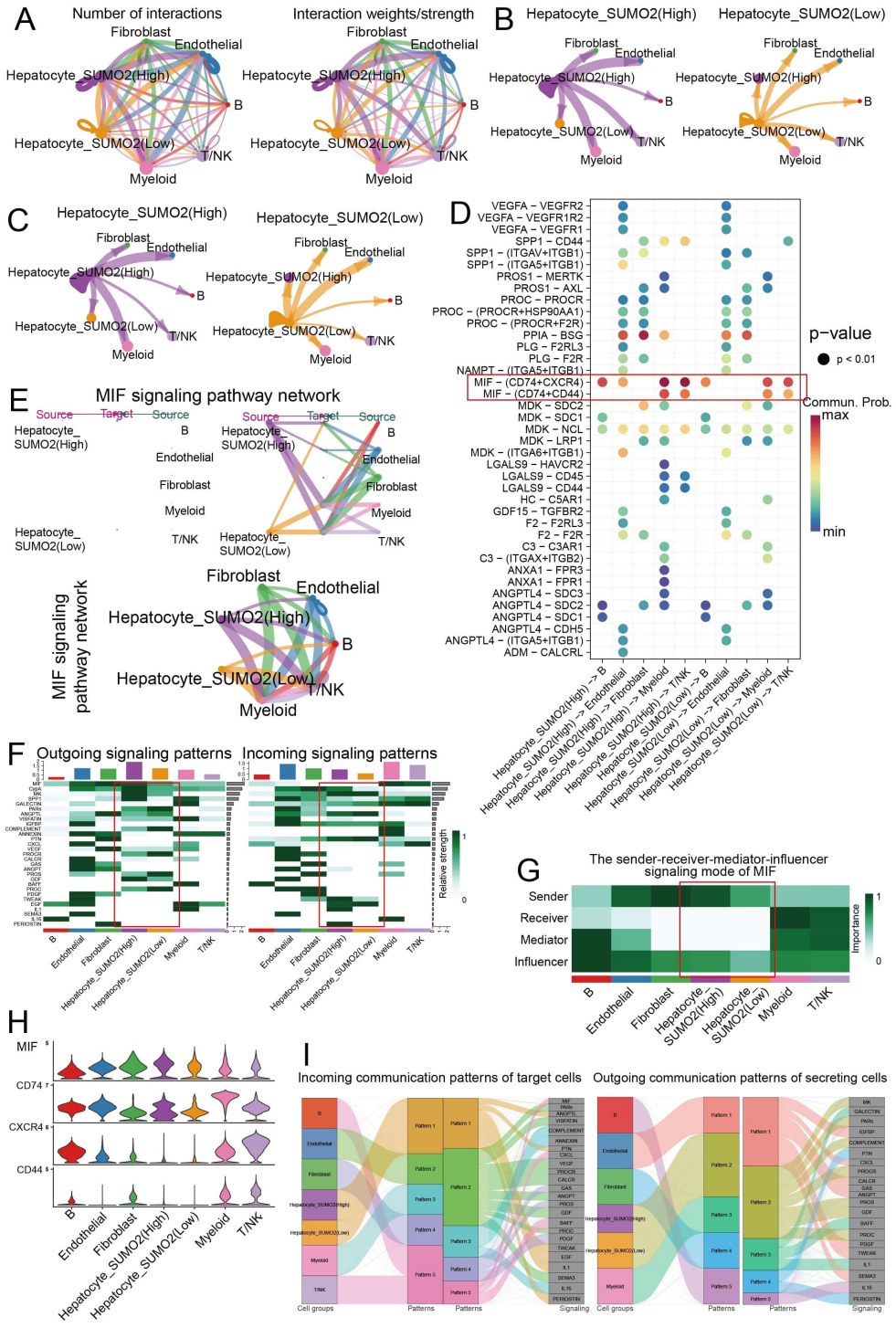

Fig. 7. Relationship between SUMO2 high- and low-expression subpopulations in hepatocytes and intercellular signaling pathways. (A) Integrated communication network among all cell types; (B) Interaction strength plot for SUMO2 high- and low-expression hepatocyte subpopulations; (C) Interaction number plot for SUMO2 high- and low-expression hepatocyte subpopulations; (D) Bubble plot of signaling pathways for interactions between SUMO2 high-/low-expression hepatocyte subpopulations and other cell types; (E) Hierarchical plot and network plot of cell interactions within the MIF signaling pathway; (F) Heatmap of incoming or outgoing signaling pathway patterns for each cell subpopulation; (G) Identification of the core contribution pattern of each cell subpopulation in the MIF signaling pathway; (H) Expression distribution of genes related to the MIF signaling pathway across cell subpopulations; (I) Other significant incoming and outgoing communication patterns for each cell type.

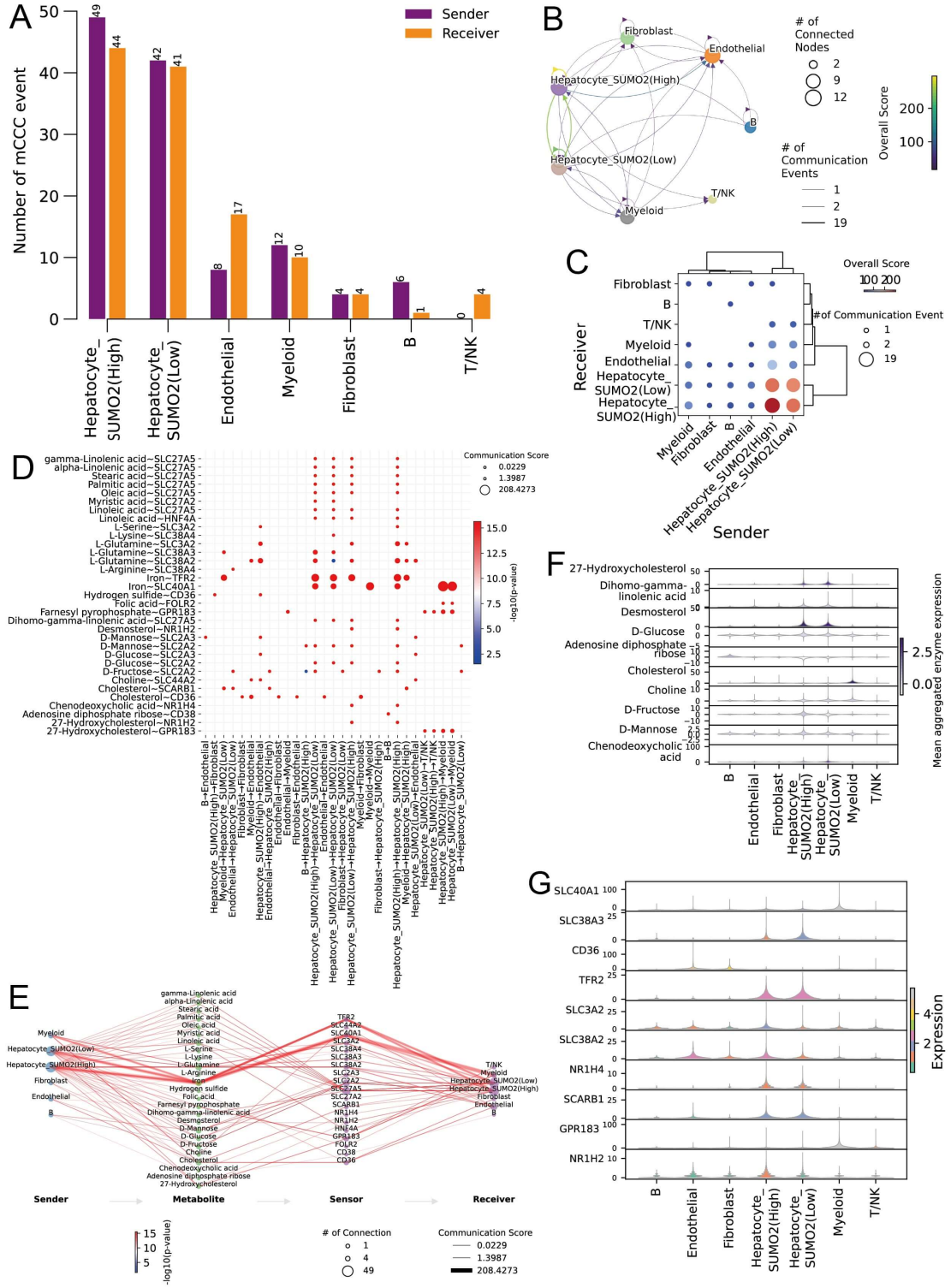

Fig. 8. Analysis of the interaction strength mediated by SUMO2 and metabolites. (A) Analysis of the number of "metabolite-sensor" ligands in each cell subpopulation; (B) Analysis of the communication strength of metabolites in each cell subpopulation; (C) Dotplot bubble plot analysis of the communication strength of metabolites in each cell subpopulation; (D) Dot plot analysis of "Sender-Receiver" interactions and metabolite sensors in each cell subpopulation; (E) Visualization analysis of the communication flow from sender-metabolite-receiver-sensor in each cell subpopulation; (F) Visualization analysis of metabolite expression in each cell group; (G) Visualization analysis of sensor expression in each cell group.

cant distribution in metabolic pathways such as glycolysis/gluconeogenesis, citrate cycle (TCA cycle), and pyruvate metabolism (**Supplementary Fig. 8A–O**). Further virtual computational analysis in the scRNA-seq dataset using scFEA revealed that the SUMO2-high group exhibited high activity in the conversion and efflux of metabolites such as M2: G6P_G3P, M5: Pyruvate_Acetyl-CoA, and M78: Lactate_Lactate_out (Fig. 9B,C).

3.11 SUMO2 Expression Exhibits Significant Differential Correlations With the HCC Immune Microenvironment

The relationship between SUMO2 high- and SUMO2-low expression groups and the immune microenvironment in HCC was systematically evaluated using the CIBERSORTx algorithm (**Supplementary Fig. 9A**). The results revealed significant differences in the association of SUMO2 expression with plasma cells, follicular helper T cells, regulatory T cells (Tregs), and M1 macrophages ($p < 0.05$; **Supplementary Fig. 9B**). Notably, a significant negative correlation was found with plasma cells and M1 macrophages ($R < 0$; **Supplementary Fig. 9C**), while a positive correlation was observed with follicular helper T cells and regulatory T cells ($R > 0$; **Supplementary Fig. 9C**).

3.12 High SUMO2 Expression Is Significantly Associated With Poor Prognosis and Clinicopathological Characteristics in HCC

The Kaplan–Meier survival analysis based on the TCGA-LIHC and GSE76427 datasets showed that patients with high SUMO2 expression had a significantly shorter overall survival than those with low SUMO2 expression ($p < 0.05$; **Supplementary Fig. 10A**). Further analysis revealed significant associations between high SUMO2 expression and older patients (age ≥65), advanced tumor stage, larger tumor size (T stage), poorly differentiated histological grade, and an increased body mass index (BMI ≥25) (all $p < 0.05$; **Supplementary Fig. 10B**).

The analysis of mutational burden revealed that compared to the low SUMO2 expression group, the high expression group exhibited significantly enhanced genomic instability. Specifically, the mutations in the key tumor suppressor genes TP53 and CSMD3 were significant, and chromosomal copy number alterations—including amplifications (e.g., 1q21.3, 1q42.2) and deletions (e.g., 1p36.23, 3p21.31)—were significantly enriched in the high expression group (**Supplementary Fig. 10C**).

3.13 High SUMO2 Expression Is Associated With Predicted Sensitivity to Multiple Drugs

The analysis of the scRNA-seq data using the scRank algorithm to model drug-SUMO2 effect activity revealed that the drug effect in SUMO2-high hepatocytes was significantly higher than in other cell populations (Fig. 10A). The GSEA analysis based on the perturbed gene set from the model drug-SUMO2 effect revealed significant enrichment in multiple key biological pathways. These include the pathways affecting drug clearance efficiency and efficacy (Hallmark Xenobiotic Metabolism), cell cycle regulation (Hallmark G2M Checkpoint and Hallmark E2F Targets), and anti-tumor mechanisms involving TORC1 (Hallmark mTORC1 Signaling) (Fig. 10B).

Based on the SUMO2 expression levels, drug sensitivity was further comprehensively evaluated using the mean R of the significant negative correlations with the IC50. The results showed that, in the GDSC2 database, Sepantronium bromide (R = –0.307694055) and Dasatinib (R = –0.148338319); in the PRISM database, BRD-K71781559 (R = –0.494781009) and IU1 (R = –0.383395451); and in the CTRP database, Aminopentamide (R = –0.595884347) and Zuclopenthixol (R = –0.571998792) all exhibited a negative correlation trend (Fig. 10C and **Supplementary Table 3**). Finally, the above candidate small-molecule drugs were subjected to molecular docking simulations with the SUMO2 protein. Among them, Dasatinib showed the most favorable predicted binding affinity (Vina score = –8.5 kcal/mol) in the docking analysis (Fig. 10D).

4. Discussion

HCC remains a significant clinical challenge due to its highly aggressive nature and poor prognosis [36]. Although several studies have preliminarily suggested at a single-omics level that aberrant SUMO2 expression may play an important role in the malignant progression of HCC, its metabolism-related mechanisms remain unclear. Building on this, our study integrated IHC experiments, large-scale bulk RNA-seq samples, scRNA-seq, ST, and CRISPR knockout data from multi-center databases. We cross-validated the high expression level of SUMO2 from the perspectives of mRNA, cells, and proteins using a combination of multiple algorithms and found that its aberrant expression may be associated with previously underexplored metabolism-related mechanisms, thereby exhibiting strong correlations with the tumor microenvironment and mutational burden.

The aberrant expression of SUMO2 may promote malignant tumor progression and is closely associated with a poor prognosis. Previous studies have shown that SUMO2 is abnormally highly expressed in various malignancies, such as gastric and colorectal cancers [37]. In HCC research, using HBV-related HCC samples and quantitative PCR technology, it has been confirmed that SUMO2 is significantly upregulated in tumor tissues [12]. Furthermore, bioinformatics analyses based on public databases and studies focusing on the regulatory network of the ubiquitin-conjugating enzyme E2I (UBE2I) consistently indicate that SUMO2 is a key marker gene for poor prognosis in HCC [11,38]. Functional experiments in two HCC cell lines, SMMC-7721 and Bel-7404, demonstrated that downregulating SUMO2 expression significantly inhibited the proliferation, migration, and invasion capabilities of liver cancer cells [11]. Another study found that inhibiting SUMO2/3

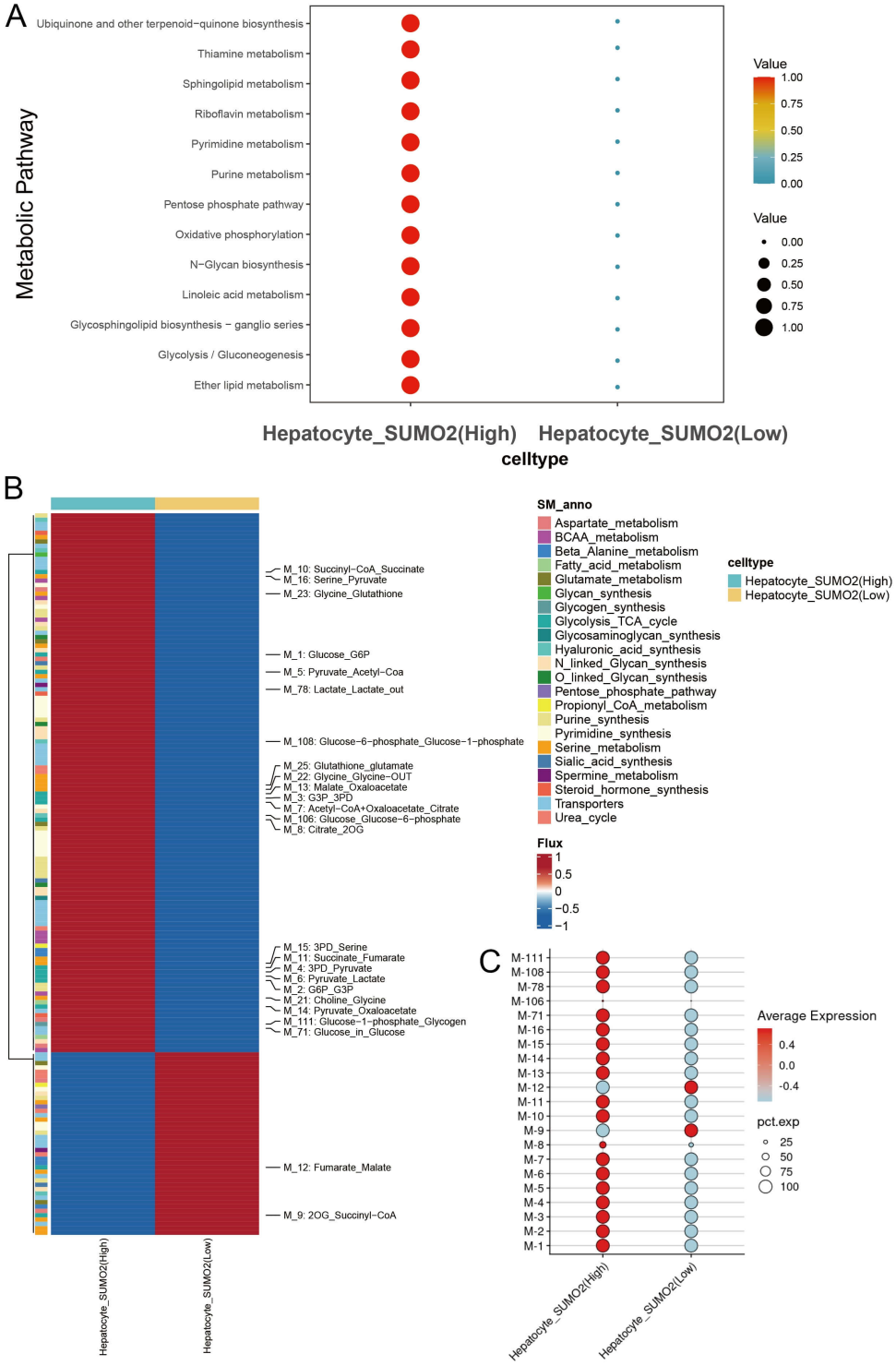

Fig. 9. Metabolic analysis associated with SUMO2 expression at the scRNA-seq level. (A) scMetabolism metabolic score analysis of SUMO2 high- and low-expression groups; (B) Metabolite conversion analysis of SUMO2 high- and low-expression groups; (C) Expression level analysis of metabolite conversion in SUMO2 high- and low-expression groups.

could counteract the tumor-promoting effects induced by isoflurane in Hep3B liver cancer cells [39]. Although this evidence preliminarily suggests the potential oncogenic role of SUMO2, the related studies are mostly based on small sample sizes or single technical approaches, thereby lacking systematic validation. This study thus integrated large-sample, multi-center bulk RNA data (5507 samples), internal pathological specimens (174 samples), and external proteomics data (318 samples). For the first time, ROC curves were employed to aid in evaluating discriminatory

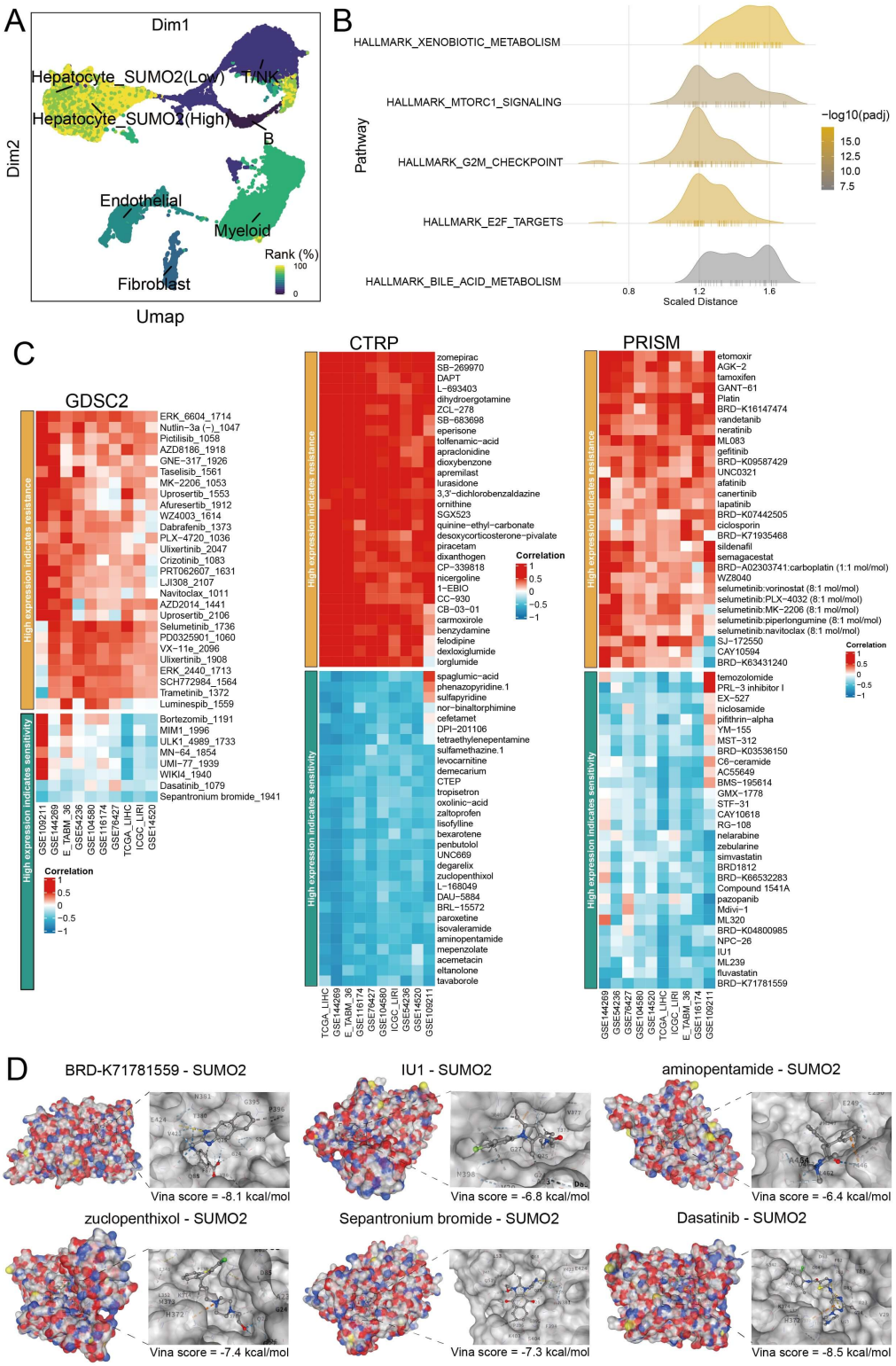

Fig. 10. Drug sensitivity analysis. (A) UMAP visualization of the Modular Drug-SUMO2 effect activity across different cell types analyzed by scRank; (B) GSEA enrichment analysis of perturbed genes associated with the Modular Drug-SUMO2 effect in malignant hepatocytes; (C) Heatmap showing the correlation between SUMO2 expression and drug sensitivity (IC50) based on GDSC, CTRP, and PRISM drug sensitivity data (Red: positive correlation; Blue: negative correlation); (D) Molecular docking analysis of candidate small-molecule drugs with the SUMO2 protein.

power, revealing that SUMO2 is significantly upregulated at both the mRNA and protein levels in HCC tissues. More importantly, by integrating scRNA-seq and ST data for the first time, our study clearly demonstrates the specific high expression of SUMO2 in malignant cells and tumor core regions. In summary, our study provides a multi-dimensional and comprehensive analysis of the SUMO2 expression profile in HCC across mRNA, proteomic, single-cell, and spatial dimensions, supporting its further investigation as a candidate prognostic biomarker and potential therapeutic target.

This study further revealed, through multi-dimensional analysis employing multiple algorithms, the impact of high SUMO2 expression on various metabolism-related pathways, with a particular focus on glucose metabolism pathways, such as glycolysis/gluconeogenesis, pyruvate metabolism, and the TCA cycle. Previous research has established that metabolic reprogramming is a key mechanism driving HCC tumor cell proliferation [40,41]. Further studies indicate that interfering with the glycolysis/gluconeogenesis pathway can effectively inhibit HCC cell survival [42], highlighting the importance of this pathway in HCC. It is particularly noteworthy that in a gastric cancer model, SUMO2 was shown to promote gastric cancer development by regulating metabolic reprogramming through the modification of ENO1 decarboxylation, thereby enhancing the binding stability between SENP1 and ENO1 [43]. Similarly, in HCC, SUMO2 has been identified as part of a lactylation-related gene set that also participates in regulating the glucose metabolism/glycolysis pathways [10], suggesting that SUMO2 may influence the metabolic state of HCC through a similar mechanism. The integrated pseudotime trajectory analysis revealed that SUMO2 expression peaks during the late developmental stage of malignant hepatocytes, and the various branches of these malignant hepatocytes are enriched in metabolism- and proliferation-related functions. This further suggests that high SUMO2 expression may be associated with the acquisition of differentiation capacity and energy by HCC cells, thereby contributing to a highly malignant phenotype.

Furthermore, the cell–cell communication analysis revealed that malignant hepatocytes with high SUMO2 expression significantly enhanced the interactions with endothelial cells, myeloid cells, and T/NK cells via the MIF-(CD74 - CXCR4)/(CD74 - CD44) signaling axis. The macrophage migration inhibitory factor (MIF), a widely expressed inflammatory cytokine, has emerged as a key mediator in the responses to infection, inflammation, and even cancer [44], influencing the immune microenvironment in various disease contexts to drive disease progression [45,46,47]. Particularly in HCC, high CD74 expression shapes the tumor microenvironment through MIF-CD74 signaling, promoting the efficacy of immunotherapy [48]. Concurrently, it has been reported that high CD44 expression can enhance the invasiveness and distant metastatic potential of HCC by inducing CXCR4 expression [49]. Further investigation into metabolite-mediated intercellular interactions revealed that SUMO2 exerts its pro-tumorigenic effects through the metabolite iron and its associated sensors (TFR2 and SLC40A1). Iron, an essential trace element for oxygen transport, DNA synthesis, and cell proliferation, plays a crucial role in HCC pathogenesis when its metabolism is dysregulated. For instance, hepatic iron overload can trigger oxidative stress, inflammatory responses, and DNA damage, thereby increasing the risk of HCC [50]. The sensor protein SLC40A1 plays a central role in cellular iron export, and its aberrant expression can disrupt intracellular iron homeostasis, promoting ferroptosis [51,52]. Similarly, the overexpression of the sensor transferrin receptor 1 (TfR1) is closely associated with tumor dedifferentiation and is considered a potential prognostic marker in HCC [53]. Additionally, the downregulation of TFR2 expression by EZH2 can inhibit the ferroptosis process in HCC and reduce sensitivity to sorafenib [54]. These findings collectively indicate that the significant association of SUMO2 with both MIF signaling and iron metabolism may be involved in the complex processes of HCC initiation and progression.

The studies by Yu-Qiang Liu, Jing Wang, and others have demonstrated that metabolic reprogramming in cancer cells drives their own proliferation as well as remodels the tumor microenvironment (TME), thereby influencing immune cell function and immune evasion [55,56]. Concurrently, Tregs are established promoters of immunosuppression [57], while the Tfh cells are enriched in various malignancies and correlate with poor prognosis [58]. M1-type macrophages, which rely on aerobic glycolysis and whose polarization is regulated by inflammatory signals, play a crucial role in anti-tumor immunity [59,60]. Integrating this evidence with our findings on cell–cell communication and immune infiltration, we hypothesize that high SUMO2 expression may be associated with altered tumor cell–immune cell interactions and metabolic abnormalities and correlated with reduced M1 macrophage infiltration and accumulation of Tfh and Tregs, which may contribute to the formation of an immunosuppressive microenvironment; however, these hypotheses require experimental validation.

The finding of multi-level high expression of SUMO2 in this study suggests potential clinical translational directions. On the one hand, its high expression is significantly correlated with poor prognosis and clinically high-risk features, such as older age, advanced stage, large tumor volume, poor differentiation, and high BMI. On the other hand, its high expression was negatively correlated with the IC50 of multiple drugs, and Dasatinib exhibited binding affinity to the SUMO2 protein in computational simulations; however, this is a computational prediction and requires experimental validation for its anti-HCC activity. Consistent with previous related studies, Dasatinib has been shown

to inhibit the growth and metastasis of HCC when combined with agents such as phenethyl isothiocyanate [61,62]. SUMO2 thus shows promise as a novel biomarker for HCC diagnosis or prognosis assessment and potentially serves as a therapeutic target.

5. Limitations

This study has certain limitations. First, its main conclusions are based on bioinformatics analyses of multicenter, large-sample, multidimensional omics data. The IHC validation performed in this study, while providing preliminary support, was conducted using a limited sample set without a multicenter or balanced cohort design. Therefore, the causal mechanisms by which SUMO2 influences immune microenvironment remodeling via metabolic reprogramming and the MIF signaling pathway have not been fully validated at the functional level. Future research should integrate *in vitro* and *in vivo* experiments to clarify the direct role of SUMO2 in mediating these key molecular mechanisms. Second, spatial transcriptomics analysis was performed on only a single sample. Therefore, the observed spatial localization patterns of SUMO2 should be interpreted as preliminary and hypothesis-generating, and any broad conclusions regarding SUMO2 spatial distribution must be drawn with caution. Independent validation using additional ST datasets is required to confirm these findings. Third, the drug sensitivity correlations (including the negative correlation between SUMO2 expression and dasatinib IC50) and the molecular docking results are purely computational predictions derived from public databases and blind docking tools. These findings do not demonstrate SUMO2-dependent drug sensitivity nor direct binding in cells. Accordingly, all drug-related conclusions should be considered hypothesis-generating rather than mechanistic. Functional validation-such as SUMO2 knockdown or overexpression combined with dasatinib treatment in HCC cell lines-is necessary to assess causal effects on drug response. Moreover, to verify the predicted binding, future experiments including competition assays (e.g., surface plasmon resonance [SPR] or cellular thermal shift assay [CETSA]) and molecular dynamics simulations are planned as part of our ongoing follow-up studies. Fourth, regarding clinical translation, the potential of SUMO2 as a prognostic biomarker or therapeutic target still requires systematic evaluation through multicenter, large-sample prospective cohort studies and drug intervention experiments.

6. Conclusion

This study suggests that the aberrant expression of SUMO2 at the bulk level and its malignant expression distribution at the single-cell and spatial levels in HCC influence metabolic reprogramming and enhance MIF signaling, thereby being highly associated with the tumor microenvironment. These findings, based on model-based computational predictions, support the potential of SUMO2 as a candidate diagnostic and therapeutic biomarker, but further experimental and clinical validation is required.

Availability of Data and Materials

The datasets during and analysed during the current study available from the corresponding author on reasonable request.

Author Contributions

YLD and BBH were responsible for the execution of the experiments, systematic analysis of the data, and drafting the initial manuscript. YXT, QYS, HQL, HBM, HHT, KHX, SPH, YWD and GC provided key assistance in optimizing the experimental design and were responsible for the rigorous implementation of data collection and statistical analysis. YLD and BBH focused on deepening the data analysis and made detailed revisions and improvements to the manuscript. MHR, as the core planner of the research, not only proposed the overall research concept but also guided the preparation and revision of the paper throughout, providing comprehensive oversight of the entire research process. All authors contributed to editorial changes in the manuscript. All authors read and approved the final manuscript. All authors have participated sufficiently in the work and agreed to be accountable for all aspects of the work.

Ethics Approval and Consent to Participate

This study was conducted in accordance with the ethical principles of the Declaration of Helsinki. The use of human tissue samples was approved by the Ethics Committee of the First Affiliated Hospital of Guangxi Medical University (Approval No.: 2020-KY-Guoji-058). Written informed consent was obtained from all patients or their legal representatives prior to participation.

Acknowledgment

We would like to thank the "Guangxi Zhuang Autonomous Region Clinical Medicine Research Center for Molecular Pathology and Intelligent Pathology Precision Diagnosis" for providing technical support, and the publicly available databases, including TCGA, GEO, ICGC, GTEx, CCLE, and PDC, for providing accessible and high-quality multi-omics data.

Funding

This work was supported by the Future Academic Star of Guangxi Medical University (WLXSZX26B029).

Conflicts of Interest

The authors declare no conflicts of interest.

Supplementary Material

Supplementary material associated with this article can be found, in the online version, at https://doi.org/10.31083/FBL52385.

References

[1] Sato-Espinoza K, Valdivia-Herrera M, Chotiprasidhi P, Diaz-Ferrer J. Hepatocellular carcinoma in patients without cirrhosis. World Journal of Gastroenterology. 2025; 31: 107100. https://doi.org/10.3748/wjg.v31.i23.107100

[2] Moris D, Martinino A, Schiltz S, Allen PJ, Barbas A, Sudan D, et al. Advances in the treatment of hepatocellular carcinoma: An overview of the current and evolving therapeutic landscape for clinicians. CA: a Cancer Journal for Clinicians. 2025; 75: 498–527. https://doi.org/10.3322/caac.70018

[3] Tabrizian P, Pero A, Schwartz M. Hepatic Resection for Hepatocellular Carcinoma. Clinics in Liver Disease. 2025; 29: 59–72. https://doi.org/10.1016/j.cld.2024.08.008

[4] Zhong BY, Fan W, Guan JJ, Peng Z, Jia Z, Jin H, et al. Combination locoregional and systemic therapies in hepatocellular carcinoma. The Lancet. Gastroenterology & Hepatology. 2025; 10: 369–386. https://doi.org/10.1016/S2468-1253(24)00247-4

[5] Singal AG, Salem R, Pinato DJ, Pillai A. Advances in Locoregional and Systemic Treatments for Hepatocellular Carcinoma. Gastroenterology. 2025; 169: 585–599. https://doi.org/10.1053/j.gastro.2025.03.047

[6] Sharma KK, Mohsin M, Mittal P, Ali Z, Fatma N, Upadhyay P, et al. Diagnosis of the Initial Stage of Hepatocellular Carcinoma: A Review. Current Pharmaceutical Design. 2024; 30: 1708–1724. https://doi.org/10.2174/0113816128298875240321073907

[7] Yang W, Nguyen R, Safri F, Shiddiky MJA, Warkiani ME, George J, et al. Liquid Biopsy in Hepatocellular Carcinoma: ctDNA as a Potential Biomarker for Diagnosis and Prognosis. Current Oncology Reports. 2025; 27: 791–802. https://doi.org/10.1007/s11912-025-01681-3

[8] Zheng W, Haw Y, Wang HL. Advances in Hepatocellular Carcinoma: Molecular Insights, Histologic Subtypes, and Differential Diagnosis. Advances in Anatomic Pathology. 2025; 32: 317–326. https://doi.org/10.1097/PAP.0000000000000501

[9] Liao Z, Steenwinkel TE, Moscoso B, Salas E, Patton BK, Rodriguez A, et al. Disruption of oocyte SUMOylation impacts critical mice†. Biology of Reproduction. 2025; 112: 932–941. https://doi.org/10.1093/biolre/ioaf035

[10] Chen Y, Chang L, Hu L, Yan C, Dai L, Shelat VG, et al. Identification of a lactylation-related gene signature to characterize subtypes of hepatocellular carcinoma using bulk sequencing data. Journal of Gastrointestinal Oncology. 2024; 15: 1636–1646. https://doi.org/10.21037/jgo-24-405

[11] Chen J, Chen C, Lin Y, Su Y, Yu X, Jiang Y, et al. Downregulation of SUMO2 inhibits hepatocellular carcinoma cell proliferation, migration and invasion. FEBS Open Bio. 2021; 11: 1771–1784. https://doi.org/10.1002/2211-5463.13173

[12] Khai NX, Huy DQ, Trang DT, Minh NT, Tien TD, Phuong NV, et al. Expression of SUMO and NF-κB genes in hepatitis B virus-associated hepatocellular carcinoma patients: An observational study. Medicine. 2024; 103: e38737. https://doi.org/10.1097/MD.0000000000038737

[13] Liu Y, Wang X, Zeng X, Wu Y, Liu X, Tan J, et al. Bioinformatics-based analysis of SUMOylation-related genes in hepatocellular carcinoma reveals a role of upregulated SAE1 in promoting cell proliferation. Open Medicine (Warsaw, Poland). 2022; 17: 1183–1202. https://doi.org/10.1515/med-2022-0510

[14] Liu J, Li X, Chen J, Guo J, Guo H, Zhang X, et al. Targeting SUMOylation with an injectable nanocomposite hydrogel to optimize radiofrequency ablation therapy for hepatocellular carcinoma. Journal of Nanobiotechnology. 2024; 22: 338. https://doi.org/10.1186/s12951-024-02579-1

[15] Shen Y, Ye B, Li C. SUMO2 inhibits ACSL3 protein degradation to antagonize erastin-induced ferroptosis in hepatocellular carcinoma. Discover Oncology. 2025; 16: 1131. https://doi.org/10.1007/s12672-025-02921-5

[16] Peng Z, Wang S, Wen D, Mei Z, Zhang H, Liao S, et al. FEN1 upregulation mediated by SUMO2 via antagonizing proteasomal degradation promotes hepatocellular carcinoma stemness. Translational Oncology. 2024; 44: 101916. https://doi.org/10.1016/j.tranon.2024.101916

[17] Liu C, Xu K, Liu J, He C, Liu P, Fu Q, et al. LncRNA RP11-620J15.3 promotes HCC cell proliferation and metastasis by targeting miR-326/GPI to enhance glycolysis. Biology Direct. 2023; 18: 15. https://doi.org/10.1186/s13062-023-00370-0

[18] Lu M, Wu Y, Xia M, Zhang Y. The role of metabolic reprogramming in liver cancer and its clinical perspectives. Frontiers in Oncology. 2024; 14: 1454161. https://doi.org/10.3389/fonc.2024.1454161

[19] Yang Y, Gao Y, Xiong Y, Gong Y, Lu J, Zhang Y, et al. Research Progress of Warburg Effect in Hepatocellular Carcinoma. Frontiers in Bioscience (Landmark Edition). 2024; 29: 178. https://doi.org/10.31083/j.fbl2905178

[20] Zeng DT, Chen ZY, Li ZYM, Chi BT, Li JD, Zhang W, et al. The Role and Mechanism of G Protein Subunit Alpha-15 in Colorectal Cancer: An Analysis of Two Hundred Eight Patient Samples and Public Datasets. World Journal of Oncology. 2026; 17: 116–128. https://doi.org/10.14740/wjon2647

[21] Chen ZD, Lu HP, Zhan YT, He FY, Zhu LQ, Deng YL, et al. Overexpression, clinical significance and potential mechanisms of protein kinase D1 in hepatocellular carcinoma: multi-omic analyses and pharmacological insights. Functional & Integrative Genomics. 2026; 26: 37. https://doi.org/10.1007/s10142-026-01825-z

[22] Jiang S, Lu H, Pan Y, Yang A, Aikemu A, Li H, et al. Characterization of the distinct immune microenvironments between hepatocellular carcinoma and intrahepatic cholangiocarcinoma. Cancer Letters. 2024; 588: 216799. https://doi.org/10.1016/j.canlet.2024.216799

[23] Virshup I, Bredikhin D, Heumos L, Palla G, Sturm G, Gayoso A, et al. The scverse project provides a computational ecosystem for single-cell omics data analysis. Nature Biotechnology. 2023; 41: 604–606. https://doi.org/10.1038/s41587-023-01733-8

[24] Gulati GS, Sikandar SS, Wesche DJ, Manjunath A, Bharadwaj A, Berger MJ, et al. Single-cell transcriptional diversity is a hallmark of developmental potential. Science (New York, N.Y.). 2020; 367: 405–411. https://doi.org/10.1126/science.aax0249

[25] Osorio D, Zhong Y, Li G, Xu Q, Yang Y, Tian Y, et al. scTenifoldKnk: An efficient virtual knockout tool for gene function predictions via single-cell gene regulatory network perturbation. Patterns (New York, N.Y.). 2022; 3: 100434. https://doi.org/10.1016/j.patter.2022.100434

[26] Xiong K, Fang Y, Qiu B, Chen C, Huang N, Liang F, et al. Investigation of cellular communication and signaling pathways in tumor microenvironment for high TP53-expressing osteosarcoma cells through single-cell RNA sequencing. Medical Oncology (Northwood, London, England). 2024; 41: 93. https://doi.org/10.1007/s12032-024-02318-4

[27] Zheng R, Zhang Y, Tsuji T, Gao X, Shamsi F, Wagner A, et al. MEBOCOST maps metabolite-mediated intercellular communications using single-cell RNA-seq. Nucleic Acids Research. 2025; 53: gkaf569. https://doi.org/10.1093/nar/gkaf569

[28] Wu Y, Yang S, Ma J, Chen Z, Song G, Rao D, et al. Spatiotemporal Immune Landscape of Colorectal Cancer Liver Metastasis at Single-Cell Level. Cancer Discovery. 2022; 12: 134–153. https://doi.org/10.1158/2159-8290.CD-21-0316

[29] Alghamdi N, Chang W, Dang P, Lu X, Wan C, Gampala S, et al. A graph neural network model to estimate cell-wise metabolic flux using single-cell RNA-seq data. Genome Research. 2021; 31: 1867–1884. https://doi.org/10.1101/gr.271205.120

[30] Li C, Shao X, Zhang S, Wang Y, Jin K, Yang P, et al. scRank infers drug-responsive cell types from untreated scRNA-seq data using a target-perturbed gene regulatory network. Cell Reports. Medicine. 2024; 5: 101568. https://doi.org/10.1016/j.xcrm.2024.101568

[31] Ru B, Huang J, Zhang Y, Aldape K, Jiang P. Estimation of cell lineages in tumors from spatial transcriptomics data. Nature Communications. 2023; 14: 568. https://doi.org/10.1038/s41467-023-36062-6

[32] Meyers RM, Bryan JG, McFarland JM, Weir BA, Sizemore AE, Xu H, et al. Computational correction of copy number effect improves specificity of CRISPR-Cas9 essentiality screens in cancer cells. Nature Genetics. 2017; 49: 1779–1784. https://doi.org/10.1038/ng.3984

[33] Sannigrahi MK, Cao AC, Rajagopalan P, Sun L, Brody RM, Raghav L, et al. A novel pipeline for prioritizing cancer type-specific therapeutic vulnerabilities using DepMap identifies PAK2 as a target in head and neck squamous cell carcinomas. Molecular Oncology. 2024; 18: 336–349. https://doi.org/10.1002/1878-0261.13558

[34] Liu Z, Liu L, Weng S, Xu H, Xing Z, Ren Y, et al. BEST: a web application for comprehensive biomarker exploration on large-scale data in solid tumors. Journal of Big Data. 2023; 10: 165. https://doi.org/10.1186/s40537-023-00844-y

[35] Tang YX, Pang YY, Cui Y, Wu GJ, Huang LQ, Zhou CZ, et al. Molecular mechanism and biological pathway of high-expressed RAD51 in regulating cell adhesion and potentially affecting oral squamous cell carcinoma. Discover Oncology. 2025; 16: 1260. https://doi.org/10.1007/s12672-025-03085-y

[36] Das J, Barman B, Sarma P, Das BK, Chetia R, Kalita PP. Signalling pathways in hepatocellular carcinoma (HCC) metastasis and invasion: Molecular mechanisms and therapeutic implications. Biochemistry and Biophysics Reports. 2025; 45: 102403. https://doi.org/10.1016/j.bbrep.2025.102403

[37] Feng D, He J, Yuan M, Chen Q, Zeng X, Zhou Q, et al. SUMO2/3 promotes the progression and oxaliplatin resistance of colorectal cancer through facilitating the SUMOylation at Ku80-K307. BioFactors (Oxford, England). 2023; 49: 1158–1173. https://doi.org/10.1002/biof.1984

[38] Yang H, Gao S, Chen J, Lou W. UBE2I promotes metastasis and correlates with poor prognosis in hepatocellular carcinoma. Cancer Cell International. 2020; 20: 234. https://doi.org/10.1186/s12935-020-01311-x

[39] Wang P, Xue N, Zhang C, Shan S, Jiang Z, Wu W, et al. Inhibition of SUMO2/3 antagonizes isoflurane-induced cancer-promoting effect in hepatocellular carcinoma Hep3B cells. Oncology Letters. 2021; 21: 274. https://doi.org/10.3892/ol.2021.12535

[40] Lin J, Rao D, Zhang M, Gao Q. Metabolic reprogramming in the tumor microenvironment of liver cancer. Journal of Hematology & Oncology. 2024; 17: 6. https://doi.org/10.1186/s13045-024-01527-8

[41] Mao Y, Xia Z, Xia W, Jiang P. Metabolic reprogramming, sensing, and cancer therapy. Cell Reports. 2024; 43: 115064. https://doi.org/10.1016/j.celrep.2024.115064

[42] Li L, Xu H, Qu L, Xu K, Liu X. Daidzin inhibits hepatocellular carcinoma survival by interfering with the glycolytic/gluconeogenic pathway through downregulation of TPI1. BioFactors (Oxford, England). 2022; 48: 883–896. https://doi.org/10.1002/biof.1826

[43] Fang Y, Gu Y, Xu T, Wang P, Wu X, Shen H, et al. SENP1 drives glycolysis and cisplatin resistance in gastric cancer via desumoylating ENO1. Journal of Experimental & Clinical Cancer Research : CR. 2025; 44: 285. https://doi.org/10.1186/s13046-025-03543-z

[44] Valdez CN, Sánchez-Zuno GA, Bucala R, Tran TT. Macrophage Migration Inhibitory Factor (MIF) and D-Dopachrome Tautomerase (DDT): Pathways to Tumorigenesis and Therapeutic Opportunities. International Journal of Molecular Sciences. 2024; 25: 4849. https://doi.org/10.3390/ijms25094849

[45] Thavayogarajah T, Sinitski D, El Bounkari O, Torres-Garcia L, Lewinsky H, Harjung A, et al. CXCR4 and CD74 together enhance cell survival in response to macrophage migration-inhibitory factor in chronic lymphocytic leukemia. Experimental Hematology. 2022; 115: 30–43. https://doi.org/10.1016/j.exphem.2022.08.005

[46] Xiao Y, Hu F, Chi Q. Single-cell RNA sequencing and spatial transcriptome reveal potential molecular mechanisms of lung cancer brain metastasis. International Immunopharmacology. 2024; 140: 112804. https://doi.org/10.1016/j.intimp.2024.112804

[47] Chen W, Yu X, Li H, Yuan S, Fu Y, Hu H, et al. Single-cell RNA-seq reveals MIF-(CD74 + CXCR4) dependent inhibition of macrophages in metastatic papillary thyroid carcinoma. Oral Oncology. 2024; 148: 106654. https://doi.org/10.1016/j.oraloncology.2023.106654

[48] Cheng J, Li J, Jiang X, Ma X, Li B, Zhai H, et al. CD74 facilitates immunotherapy response by shaping the tumor microenvironment of hepatocellular carcinoma. Molecular Medicine (Cambridge, Mass.). 2024; 30: 116. https://doi.org/10.1186/s10020-024-00884-x

[49] Xie P, Yan J, Wu M, Li H, Chen Z, Yu M, et al. CD44 potentiates hepatocellular carcinoma migration and extrahepatic metastases via the AKT/ERK signaling CXCR4 axis. Annals of Translational Medicine. 2022; 10: 689. https://doi.org/10.21037/atm-22-2482

[50] Rah B, Farhat NM, Hamad M, Muhammad JS. JAK/STAT signaling and cellular iron metabolism in hepatocellular carcinoma: therapeutic implications. Clinical and Experimental Medicine. 2023; 23: 3147–3157. https://doi.org/10.1007/s10238-023-01047-8

[51] Zheng J, Liu Y, Zhu F, Liu S, Cai Z, Liu M, et al. Piropodophyllin induces ferroptosis via blockage of AKT/NRF2/SLC7A11 and AKT/NRF2/SLC40A1 axes in hepatocellular carcinoma as a natural IGF1R inhibitor. Phytomedicine : International Journal of Phytotherapy and Phytopharmacology. 2025; 143: 156840. https://doi.org/10.1016/j.phymed.2025.156840

[52] Zhang Y, Zou L, Li X, Guo L, Hu B, Ye H, et al. SLC40A1 in iron metabolism, ferroptosis, and disease: A review. WIREs Mechanisms of Disease. 2024; 16: e1644. https://doi.org/10.1002/wsbm.1644

[53] Adachi M, Kai K, Yamaji K, Ide T, Noshiro H, Kawaguchi A, et al. Transferrin receptor 1 overexpression is associated with tumour de-differentiation and acts as a potential prognostic indicator of hepatocellular carcinoma. Histopathology. 2019; 75: 63–73. https://doi.org/10.1111/his.13847

[54] Lai Y, Han X, Xie B, Xu Y, Yang Z, Wang D, et al. EZH2 suppresses ferroptosis in hepatocellular carcinoma and reduces sorafenib sensitivity through epigenetic regulation of TFR2. Cancer Science. 2024; 115: 2220–2234. https://doi.org/10.1111/cas.16186

[55] Wang J, He Y, Hu F, Hu C, Sun Y, Yang K, et al. Metabolic Reprogramming of Immune Cells in the Tumor Microenvironment. International Journal of Molecular Sciences. 2024; 25: 12223. https://doi.org/10.3390/ijms252212223

[56] Liu Y, Zhao Y, Song H, Li Y, Liu Z, Ye Z, et al. Metabolic reprogramming in tumor immune microenvironment: Impact on

immune cell function and therapeutic implications. Cancer Letters. 2024; 597: 217076. https://doi.org/10.1016/j.canlet.2024.217076

[57] Zheng L, Wu D, Xie H, Zhao H. Revisiting Tregs in cancer and beyond: immunological control and therapeutic potential. Frontiers in Immunology. 2025; 16: 1581093. https://doi.org/10.3389/fimmu.2025.1581093

[58] Gutiérrez-Melo N, Baumjohann D. T follicular helper cells in cancer. Trends in Cancer. 2023; 9: 309–325. https://doi.org/10.1016/j.trecan.2022.12.007

[59] Bai X, Guo YR, Zhao ZM, Li XY, Dai DQ, Zhang JK, et al. Macrophage polarization in cancer and beyond: from inflammatory signaling pathways to potential therapeutic strategies. Cancer Letters. 2025; 625: 217772. https://doi.org/10.1016/j.canlet.2025.217772

[60] Li M, Yang Y, Xiong L, Jiang P, Wang J, Li C. Metabolism, metabolites, and macrophages in cancer. Journal of Hematology & Oncology. 2023; 16: 80. https://doi.org/10.1186/s13045-023-01478-6

[61] Strusi G, Suelzu CM, Weldon S, Giffin J, Münsterberg AE, Bao Y. Combination of Phenethyl Isothiocyanate and Dasatinib Inhibits Hepatocellular Carcinoma Metastatic Potential through FAK/STAT3/Cadherin Signalling and Reduction of VEGF Secretion. Pharmaceutics. 2023; 15: 2390. https://doi.org/10.3390/pharmaceutics15102390

[62] Strusi G, Suelzu CM, Horwood N, Münsterberg AE, Bao Y. Phenethyl isothiocyanate and dasatinib combination synergistically reduces hepatocellular carcinoma growth via cell cycle arrest and oxeiptosis. Frontiers in Pharmacology. 2023; 14: 1264032. https://doi.org/10.3389/fphar.2023.1264032